Research Article

Adaptive High-Order Finite Difference Analysis of 2D Quenching-Type Convection-Reaction-Diffusion Equation

Xiaoliang Zhu [1,2] **and Yongbin Ge** [1]

[1]*Institute of Applied Mathematics and Mechanics, Ningxia University, Yinchuan 750021, China*
[2]*School of Computer and Engineering, North Minzu University, Yinchuan 750021, China*

Correspondence should be addressed to Yongbin Ge; gyb@nxu.edu.cn

Quenching characteristics based on the two-dimensional (2D) nonlinear unsteady convection-reaction-diffusion equation are creatively researched. The study develops a 2D compact finite difference scheme constructed by using the first and the second central difference operator to approximate the first-order and the second-order spatial derivative, Taylor series expansion rule, and the reminder-correction method to approximate the three-order and the four-order spatial derivative, respectively, and the forward difference scheme to discretize temporal derivative, which brings the accuracy resulted meanwhile. Influences of degenerate parameter, convection parameter, and the length of the rectangle definition domain on quenching behaviors and performances of special quenching cases are discussed and evaluated by using the proposed scheme on the adaptive grid. It is feasible for the paper to offer potential support for further research on quenching problem.

1. Introduction

As a common class of thermodynamic problems, quenching phenomena research has been widely applied in engineering area. There exist some typical researches including the flow, thermal properties, and its working mechanism of an object in heat associated with quenching phenomena [1, 2], the forced convection quench of hot sheets in super-cooled liquid [3], the quench process speed-up, and its quench characteristics in porous interface processing [4, 5]. In recent years, more and more scholars concern quenching problem built on parabolic equations [6–10], in which the authors depended on the different parabolic equations to analyze corresponding quench features. Additionally, quenching phenomena based on parabolic equation systems have attracted researchers' attentions [11–13]. Nonlinear degeneration singularity reaction-diffusion equations or convection-reaction-diffusion equations, as a branch of parabolic equations, have been usually employed to handle quenching problems. References [14–16] focused on the quench-

ing phenomena of the nonlinear degeneration singularity reaction-diffusion equations whereas Refs. [17, 18] focused on the quenching phenomena of the nonlinear degeneration singularity convection-reaction-diffusion equations. Selcuk discussed quench performances of solution and its time derivative and estimation of quenching time under special conditions [14]. Ge et al. devoted to an adaptive compact difference scheme to solve quench problems [15]. Beauregard analyzed quenching properties of the fractional Kawarada equation by using a new numerical method and proved the proposed method monotonic, nonnegative, and linearly stable [16]. Zhou et al. theoretically investigated quenching characteristics of the nonlinear degeneration singularity convection-reaction-diffusion equation [17]. Zhu and Rui constructed a high-accuracy method with adaptation mechanism for studying quenching behaviors and analyzed the influence of important elements on quenching [18].

References [6–18] concentrated on the quenching phenomena of the 1D heat equations. The quenching phenomena of the 2D heat equations are described as follows.

References [19–21] used numerical method with adaptive algorithm to research degeneration singularity problem of the two-dimensional nonlinear reaction-diffusion equations. A Peaceman-Rachford finite difference scheme based on semi-adaptive grids with stability and convergence under certain condition was posed to analyze the quenching behaviors of the 2D reaction-diffusion equation in Ref. [19]. Numerical analyses showed that the method is very efficient and reliable. An adaptive Peaceman-Rachford-Strang splitting method on exponentially evolving meshes was constructed to resolve the 2D problem of quenching type in Ref. [20]. Computational experiments stated that the method is of the satisfactory effectiveness, efficiency, and numerical stability. An exponential splitting method with spatial semidiscretization on arbitrary nonuniform meshes was investigated to explore the 2D degenerate stochastic Kawarada equation in Ref. [21]. Zhu and Ge developed an adaptive ADI strategy to simulate quenching phenomena based on 2D convection-reaction-diffusion equation [22]. Numerical cases illustrated that the method is of the positivity, monotonicity, and numerical stability. The low-accuracy strategies were adopted in the most aforementioned researches [6–15, 19–21]. There are only Refs. [15, 18, 22] delivering the high-accuracy strategies, in which the first two refer to the one-dimensional problem and the last one refers to the two-dimensional problem. It is well known that the development of high-order finite difference scheme of the 2D nonlinear convection-reaction-diffusion equations is maturing [23–25]. Reference [23] developed a new high-order difference approach for the 2D convection-reaction-diffusion equation with a small diffusivity, which firstly posed the 1D high-accuracy difference scheme and then extended it to the 2D case a nine-point stencil by using alternating direction algorithm and last resolve the 2D steady incompressible Navier-Stokes equations. In order to simulate groundwater pollution problems, Li et al. put forward a fourth-order compact difference scheme with unconditional stability and the second-order temporal accuracy, the fourth-order spatial accuracy built on the 2D convection-reaction-diffusion model, which was efficient through experiments [24]. Wu and Zhai combined exponential transformation and quadratic interpolation polynomial with Padé approximation to study the 2D time-fractional convection-dominated diffusion equation, which owned the higher accuracy and used alternating direction implicit algorithm to alleviate computational amount [25].

In summary, it is easily found that there are much more low-order strategies than high-order strategies to solve degenerate singularity problems of the 2D reaction-diffusion equation. Especially, high-order difference schemes received few attentions for solving quenching problem of the two-dimensional convection-reaction-diffusion equation. It is the high-precision algorithms that have advantages in dealing with such problems because of its high accuracy and efficiency. So it is a meaningful try to explore the high-order compact difference schemes on adaptation mesh for analyzing quenching problems of the 2D degenerate singular reaction-diffusion equation with convection function. Going down this idea, we extend this study from Ref. [18] and construct a compact difference scheme on adaptive grid for solving the 2D unsteady convection-reaction-diffusion equation

to explain the corresponding quenching phenomena. According to Ref. [18], we extend its 1D high-order compact finite difference scheme on adaptive mesh to a 2D strategy and use it to analyze the quenching behaviors of the 2D convection-reaction-diffusion combustion model. There exist three contributions of this paper. Firstly, we represent a new 2D high-order compact difference scheme for solving the corresponding unsteady convection-reaction-diffusion equation and give its accuracy performances. Secondly, we apply the scheme to explain the 2D reaction-diffusion of quenching type with and without convection function, respectively. Thirdly, we investigate a series of quenching characteristics including quenching time, quenching location, and so on, from which we can discover impacts of the parameters q, b, and α (β) on quenching behaviors. There are five parts in the paper. Section 1 introduces the theme of this study. Section 2 describes carefully the proposed scheme of high-order accuracy. Section 3 introduces adaptive mesh algorithm. Section 4 stimulates some typical numerical samples to explore and explain quenching problems. Section 5 draws the conclusion.

2. 2D Problem and Difference Scheme

2.1. 2D Nonlinear Convection-Reaction-Diffusion Equation.
The typical convection-reaction-diffusion equation of quenching type is written as

$$\sigma(x, y)u_t = u_{xx} + u_{yy} + c_1(x, y)u_x + c_2(x, y)u_y \\ + f(u), (x, y) \in \Omega, t \in (0, T). \tag{1}$$

Its boundary conditions are

$$u(0, y, t) = u(\alpha, y, t) = u(x, 0, t) = u(x, \beta, t) = 0, t \in (0, T). \tag{2}$$

Its initial conditions is

$$u(x, y, 0) = u_0(x, y), (x, y) \in 0, \alpha) \times (0, \beta). \tag{3}$$

This semilinear degenerate problem model involving two spatial dimensions is regarded as Eq. (1) with the boundary and initial conditions of Eqs. (2) and (3). The solution $u(x, y, t)$ represents the temperature of the combustion chamber. $\Omega \in (0, \alpha) \times (0, \beta)$ refers to the smooth domain of the rectangle combustor in which $\alpha > 0$, $\beta > 0$, and combustion chamber sizes α and β are the length of the definition area, $\partial\Omega$, and is its boundary. $c_1(x, y)$ and $c_2(x, y)$ are the convection functions of x and y, and $\sigma(x, y) = (x^2 + y^2)^{q/2}$ is the degeneracy function and degeneration parameter $q \geq 0$. The singularity source $f(u) = 1/(1 - u)^\theta$ is strictly increasing for $0 \leq u_0 < 1$ with $f(0) = f_0 > 0$, $\lim_{u \to 1} f(u) = \infty$, and singularity parameter θ is the power of the singular source term $1/(1 - u)^\theta$.

With the aid of the intermediate variables $\hat{x}$ and $\hat{y}$, we replace $\hat{x} = x/\alpha$ and $\hat{y} = y/\beta$ into Eq. (1) which can be defined as

$$\sigma(\alpha\hat{x}, \beta\hat{y})u_t = \frac{1}{\alpha^2}u_{\hat{x}\hat{x}} + \frac{1}{\beta^2}u_{\hat{y}\hat{y}} + \frac{c_1(\alpha\hat{x}, \beta\hat{y})}{\alpha}u_{\hat{x}} + \frac{c_2(\alpha\hat{x}, \beta\hat{y})}{\beta}u_{\hat{y}}$$
$$+ f(u), (\alpha\hat{x}, \beta\hat{y}) \in \Omega, t \in (0, T).$$
$$(4)$$

For the convenience of expression, we use x and y instead of $\hat{x}$ and $\hat{y}$. Then, the above formulation can be rearranged as

$$\sigma(x, y)u_t = \frac{1}{\alpha^2}u_{xx} + \frac{1}{\beta^2}u_{yy} + \frac{c_1(x, y)}{\alpha}u_x + \frac{c_2(x, y)}{\beta}u_y$$
$$+ f(u), (x, y) \in \Omega, t \in (0, T), \quad (5)$$

where $\sigma(x, y) = (\alpha^2 x^2 + \beta^2 y^2)^{q/2}$, $\Omega \in (0, 1) \times (0, 1)$. Correspondingly, the boundary conditions of Eq. (5) are

$$u(0, y, t) = u(1, y, t) = u(x, 0, t) = u(x, 1, t) = 0, t \in (0, T).$$
$$(6)$$

The initial conditions of Eq. (5) is

$$u(x, y, 0) = u_0(x, y), (x, y) \in (0, 1) \times (0, 1). \quad (7)$$

In the physical application, we rely on Eqs. (5)–(7) to compute u and u_t. Through observing a large number of values of u and u_t, we can capture quenching moment, i.e., quenching occurs when u infinitely close to 1 and u_t becomes so huge that its value blows up.

2.2. The Proposed Compact Difference Scheme. According to the idea given in [18], we employ the first and the second central difference operator to approximate the first-order and the second-order spatial derivatives of x – direction and y – direction, respectively, and the forward difference operator to discrete temporal derivative. The proposed high-accuracy finite difference scheme of Eq. (5) is deduced below. After the first-order and the second-order spatial derivatives of x – direction and y – direction are discretized on the nonuniform mesh, respectively, a scheme approximating the 2D unsteady convection-diffusion equation dispersed at point (x_k, y_j) can be written as

$$\left\{ \frac{2 - \alpha(x_R - x_L)c_1}{2\alpha^2\sigma}\delta_x^2 + \frac{c_1}{\alpha\sigma}\delta_x + \frac{2 - \beta(y_R - y_L)c_2}{2\beta^2\sigma}\delta_y^2 \right.$$
$$\left. + \frac{c_2}{\beta\sigma}\delta_y \right\}u_{k,j} + \Psi_{1x}(u_{xxx})_{k,j} + \Psi_{2x}(u_{xxxx})_{k,j} + \Psi_{3x}(u_{xxxxx})_{k,j}$$
$$+ \Psi_{1y}(u_{yyy})_{k,j} + \Psi_{2y}(u_{yyyy})_{k,j} + \Psi_{3y}(u_{yyyyy})_{k,j}$$
$$= \left\{ u_t - \frac{f}{\sigma}(u) \right\}_{k,j,l} + O\left(\frac{x_R^5 + x_L^5}{x_R + x_L} \right) + O\left(\frac{y_R^5 + y_L^5}{y_R + y_L} \right),$$
$$(8)$$

where

$$\Psi_{1x} = -\frac{2(x_R - x_L) + \alpha x_R x_L c_1}{6\alpha^2\sigma},$$

$$\Psi_{2x} = -\frac{2(x_R^2 - x_R x_L + x_L^2) + \alpha(x_R - x_L)x_R x_L c_1}{24\alpha^2\sigma},$$

$$\Psi_{3x} = -\frac{2(x_R - x_L)(x_R^2 + x_L^2) + \alpha(x_R^3 x_L - x_R^2 x_L^2 + x_L^3 x_R)c_1}{120\alpha^2\sigma},$$

$$\Psi_{1y} = -\frac{2(y_R - y_L) + \beta y_R y_L c_2}{6\beta^2\sigma},$$

$$\Psi_{2y} = -\frac{2(y_R^2 - y_R y_L + y_L^2) + \beta(y_R - y_L)y_R y_L c_2}{24\beta^2\sigma},$$

$$\Psi_{3y} = -\frac{2(y_R - y_L)(y_R^2 + y_L^2) + \beta(y_R^3 y_L - y_R^2 y_L^2 + y_L^3 y_R)c_2}{120\beta^2\sigma}.$$
$$(9)$$

We use Taylor series to obtain the derivative expansions of x – direction: $(u_{xxx})_{k,j}$ and $(u_{xxxx})_{k,j}$, and the derivative expansions of y – direction: $(u_{yyy})_{k,j}$ and $(u_{yyyy})_{k,j}$ from Eq. (5). The four expressions are substituted into the corresponding terms in Eq. (8). $O(\Delta) = O(x_R^5 + x_L^5/x_R + x_L) + O(y_R^5 + y_L^5/y_R + y_L) - \Psi_{2y}(u_{yyyy})_{k,j} - \Psi_{3y}(u_{yyyyy})_{k,j}$, which is the truncation error of Eq. (8). Omitting the truncation errors, we consider the situation of point (k, j, n) for Eq. (8)

$$\left\{ \kappa_{1x}\delta_x + \kappa_{2x}\delta_x^2 + \kappa_{1y}\delta_y + \kappa_{2y}\delta_y^2 \right\}u_{k,j}^n + \left\{ \kappa_3 u_t + \kappa_{4x}u_{tx} + \kappa_{5x}u_{txx} \right.$$
$$\left. + \kappa_{4y}u_{ty} + \kappa_{5y}u_{tyy} + \kappa_6 u_{xy} + \kappa_{7x}u_{xxy} + \kappa_{7y}u_{xyy} + \kappa_8 u_{xxyy} \right\}_{k,j}^n$$
$$= \left\{ -\frac{1}{\sigma} + \kappa_{9x}\delta_x + \kappa_{10x}\delta_x^2 + \kappa_{9y}\delta_y + \kappa_{10y}\delta_y^2 \right\}f_{k,j}^n + O(\Delta),$$
$$(10)$$

where

$$\kappa_{1x} = \frac{c_1}{\alpha\sigma} - \alpha(\Psi_{1x} - \alpha\Psi_{2x}c_1)(c_1)_x - \alpha\Psi_{2x}(c_1)_{xx}$$
$$- \frac{\beta^2}{\alpha}(\Psi_{1y} - \beta\Psi_{2y}c_2)(c_1)_y - \frac{\beta^2\Psi_{2y}}{\alpha}(c_1)_{yy},$$

$$\kappa_{2x} = \frac{2 - \alpha(x_R - x_L)c_1}{2\alpha^2\sigma} - \alpha(\Psi_{1x} - \alpha\Psi_{2x}c_1)c_1 - 2\alpha\Psi_{2x}(c_1)_x,$$

$$\kappa_{1y} = \frac{c_2}{\beta\sigma} - \beta(\Psi_{1y} - \beta\Psi_{2y}c_2)(c_2)_y - \beta\Psi_{2y}(c_2)_{yy}$$
$$- \frac{\alpha^2}{\beta}(\Psi_{1x} - \alpha\Psi_{2x}c_1)(c_2)_x - \frac{\alpha^2\Psi_{2x}}{\beta}(c_2)_{xx},$$

$$\kappa_{2y} = \frac{2 - \beta(y_R - y_L)c_2}{2\beta^2\sigma} - \beta(\Psi_{1y} - \beta\Psi_{2y}c_2)c_2 - 2\beta\Psi_{2y}(c_2)_y,$$

$$\kappa_3 = \alpha^2(\Psi_{1x} - \alpha\Psi_{2x}c_1)\sigma_x + \alpha^2\Psi_{2x}\sigma_{xx}$$
$$+ \beta^2\left(\Psi_{1y} - \beta\Psi_{2y}c_2\right)\sigma_y + \beta^2\Psi_{2y}\sigma_{yy} - 1,$$

$$\kappa_{4x} = \alpha^2(\Psi_{1x} - \alpha\Psi_{2x}c_1)\sigma + 2\alpha^2\Psi_{2x}\sigma_x, \kappa_{4y}$$
$$= \beta^2\left(\Psi_{1y} - \beta\Psi_{2y}c_2\right)\sigma + 2\beta^2\Psi_{2y}\sigma_y,$$

$$\kappa_{5x} = \alpha^2\Psi_{2x}\sigma, \kappa_{5y} = \beta^2\Psi_{2y}\sigma,$$

$$\kappa_6 = -\frac{\alpha^2}{\beta}(\Psi_{1x} - \alpha\Psi_{2x}c_1)c_2 - \frac{2\alpha^2\Psi_{2x}}{\beta}(c_2)_x$$
$$- \frac{\beta^2}{\alpha}\left(\Psi_{1y} - \beta\Psi_{2y}c_2\right)c_1 - \frac{2\beta^2\Psi_{2y}}{\alpha}(c_1)_y,$$

$$\kappa_{7x} = -\frac{\alpha^2\Psi_{2x}}{\beta}c_2 - \frac{\beta^2}{\alpha^2}\left(\Psi_{1y} - \beta\Psi_{2y}c_2\right),$$

$$\kappa_{7y} = -\frac{\beta^2\Psi_{2y}}{\alpha}c_1 - \frac{\alpha^2}{\beta^2}(\Psi_{1x} - \alpha\Psi_{2x}c_1),$$

$$\kappa_8 = -\frac{\alpha^2\Psi_{2x}}{\beta^2} - \frac{\beta^2\Psi_{2y}}{\alpha^2},$$

$$\kappa_{9x} = \alpha^2(\Psi_{1x} - \alpha\Psi_{2x}c_1), \kappa_{9y} = \beta^2\left(\Psi_{1y} - \beta\Psi_{2y}c_2\right),$$

$$\kappa_{10x} = \alpha^2\Psi_{2x}, \kappa_{10y} = \beta^2\Psi_{2y}. \qquad (11)$$

The second-order derivative of time from Eq. (8) is u_{tt} $= (1/\alpha^2\sigma)u_{txx} + (1/\beta^2\sigma)u_{tyy} + (c_1/\alpha\sigma)u_{tx} + (c_2/\beta\sigma)u_{ty} + (f_t/\sigma)$. By using the forward difference scheme, we can get

$$(u_t)_{k,j}^n = \frac{u_{k,j}^{n+1} - u_{k,j}^n}{\tau_n} - \frac{\tau_n}{2}(u_{tt})_{k,j}^n + O(\tau^2)$$
$$= \delta_t^+ u_{k,j}^n - \frac{\tau_n}{2}(u_{tt})_{k,j}^n + O(\tau^2). \qquad (12)$$

Relying on the second-order backward Euler difference scheme, we can get

$$(f_t)_{k,j}^n = \frac{3f_{k,j}^n - 4f_{k,j}^{n-1} + f_{k,j}^{n-2}}{2\tau_n}. \qquad (13)$$

Provided $O(\Delta) = O(\Delta + \tau^2)$, Eq. (14) can be derived as

$$\left\{\kappa_{1x}\delta_x + \kappa_{2x}\delta_x^2 + \kappa_{1y}\delta_y + \kappa_{2y}\delta_y^2\right\}u_{k,j}^n + \kappa_3\delta_t^+ u_{k,j}^n$$
$$+ \left\{\left(\kappa_{4x} - \frac{\kappa_3\tau_nc_1}{2\alpha\sigma}\right)u_{tx} + \left(\kappa_{5x} - \frac{\kappa_3\tau_n}{2\alpha^2\sigma}\right)u_{txx}\right.$$
$$+ \left.\left(\kappa_{4y} - \frac{\kappa_3\tau_nc_2}{2\beta\sigma}\right)u_{ty} + \left(\kappa_{5y} - \frac{\kappa_3\tau_n}{2\beta^2\sigma}\right)u_{tyy}\right\}_{k,j}^n$$
$$+ \left\{\kappa_6 u_{xy} + \kappa_{7x}u_{xxy} + \kappa_{7y}u_{xyy} + \kappa_8 u_{xxyy}\right\}_{k,j}^n \qquad (14)$$
$$= \left\{-\frac{1}{\sigma} + \kappa_{9x}\delta_x + \kappa_{10x}\delta_x^2 + \kappa_{9y}\delta_y + \kappa_{10y}\delta_y^2\right\}f_{k,j}^n$$
$$+ \frac{3\kappa_3}{4\sigma}f_{k,j}^n - \frac{\kappa_3}{\sigma}f_{k,j}^{n-1} + \frac{\kappa_3}{4\sigma}f_{k,j}^{n-2} + O(\Delta).$$

The first-order and the second-order derivate of u with regard to space variables x and y are discretized by the central difference scheme. The first-order derivate of u with regard to time variable t is discretized by the forward difference scheme. Subsequently, after the difference approximations are carried out to $(u_{tx})_{k,j}^n$, $(u_{txx})_{k,j}^n$, $(u_{ty})_{k,j}^n$, $(u_{tyy})_{k,j}^n$, $(u_{xy})_{k,j}^n$, $(u_{xxy})_{k,j}^n$, $(u_{xyy})_{k,j}^n$, and $(u_{xxyy})_{k,j}^n$, a linear system is formed as

$$b_{1y}u_{k,j-1}^{n+1} + b_{1x}u_{k-1,j}^{n+1} + b_0u_{k,j}^{n+1} + b_{2x}u_{k+1,j}^{n+1} + b_{2y}u_{k,j+1}^{n+1}$$
$$= d_{1y}u_{k,j-1}^n + d_{1x}u_{k-1,j}^n + d_0u_{k,j}^n + d_{2x}u_{k+1,j}^n$$
$$+ d_{2y}u_{k,j+1}^n + d_{31}u_{k-1,j-1}^n + d_{32}u_{k+1,j-1}^n + d_{33}u_{k-1,j+1}^n$$
$$+ d_{34}u_{k+1,j+1}^n + s_{1y}f_{k,j-1}^n + s_{1x}f_{k-1,j}^n + s_0f_{k,j}^n$$
$$+ s_{2x}f_{k+1,j}^n + s_{2y}f_{k,j+1}^n + M_1f_{k,j}^{n-1} + M_2f_{k,j}^{n-2},$$

$$(15)$$

where

$$b_{1y} = \frac{(-2\tau_n + \beta c_2\tau_n y_L)\kappa_3 - 2\beta^2\sigma y_L\kappa_{4y} + 4\beta^2\sigma\kappa_{5y}}{2\beta^2\sigma\tau_n y_L(y_R + y_L)},$$

$$b_{1x} = \frac{(2\tau_n + \alpha c_1\tau_n x_L)\kappa_3 - 2\alpha^2\sigma x_L\kappa_{4x} + 4\alpha^2\sigma\kappa_{5x}}{2\alpha^2\sigma\tau_n x_L(x_R + x_L)},$$

$$b_0 = \frac{\kappa_3}{\tau_n} - \frac{2\alpha^2\sigma\kappa_{5x} - \tau_n\kappa_3}{\alpha^2\sigma\tau_n x_R x_L} - \frac{2\beta^2\sigma\kappa_{5y} - \tau_n\kappa_3}{\beta^2\sigma\tau_n y_R y_L},$$

$$b_{2x} = \frac{(-2\tau_n - \alpha c_1\tau_n x_R)\kappa_3 + 2\alpha^2\sigma x_R\kappa_{4x} + 4\alpha^2\sigma\kappa_{5x}}{2\alpha^2\sigma\tau_n x_R(x_R + x_L)},$$

$$b_{2y} = \frac{(-2\tau_n - \beta c_2\tau_n y_R)\kappa_3 + 2\beta^2\sigma y_R\kappa_{4y} + 4\beta^2\sigma\kappa_{5y}}{2\beta^2\sigma\tau_n y_R(y_R + y_L)},$$

$$d_{1y} = \frac{\kappa_{1y}}{y_R + y_L} - \frac{2\kappa_{2y}}{y_L(y_R + y_L)}$$
$$+ \frac{(-2\tau_n + \beta c_2 \tau_n y_L)\kappa_3 - 2\beta^2 \sigma y_L \kappa_{4y} + 4\beta^2 \sigma \kappa_{5y}}{2\beta^2 \sigma \tau_n y_L(y_R + y_L)}$$
$$- \frac{2\kappa_{7x}}{x_R x_L(y_R + y_L)} + \frac{4\kappa_8}{x_R x_L y_L(y_R + y_L)},$$

$$d_{1x} = \frac{\kappa_{1x}}{x_R + x_L} - \frac{2\kappa_{2x}}{x_L(x_R + x_L)}$$
$$+ \frac{(-2\tau_n + \alpha c_1 \tau_n x_L)\kappa_3 - 2\alpha^2 \sigma x_L \kappa_{4x} + 4\alpha^2 \sigma \kappa_{5x}}{2\alpha^2 \sigma \tau_n x_L(x_R + x_L)}$$
$$- \frac{2\kappa_{7y}}{(x_R + x_L)y_R y_L} + \frac{4\kappa_8}{x_L(x_R + x_L)y_R y_L},$$

$$d_0 = \frac{2\kappa_{2x}}{x_R x_L} + \frac{2\kappa_{2y}}{y_R y_L} + \frac{\kappa_3}{\tau_n} - \frac{2\alpha^2 \sigma \kappa_{5x} - \tau_n \kappa_3}{\alpha^2 \sigma \tau_n x_R x_L}$$
$$- \frac{2\beta^2 \sigma \kappa_{5y} - \tau_n \kappa_3}{\beta^2 \sigma \tau_n y_R y_L} - \frac{4\kappa_8}{x_R x_L y_R y_L},$$

$$d_{2x} = \frac{\kappa_{1x}}{x_R + x_L} - \frac{2\kappa_{2x}}{x_R(x_R + x_L)}$$
$$\cdot \frac{(-2\tau_n - \alpha c_1 \tau_n x_R)\kappa_3 + 2\alpha^2 \sigma x_R \kappa_{4x} + 4\alpha^2 \sigma \kappa_{5x}}{2\alpha^2 \sigma \tau_n x_R(x_R + x_L)}$$
$$+ \frac{2\kappa_{7y}}{(x_R + x_L)y_R y_L} + \frac{4\kappa_8}{x_R(x_R + x_L)y_R y_L},$$

$$d_{2y} = -\frac{\kappa_{1y}}{y_R + y_L} - \frac{2\kappa_{2y}}{y_R(y_R + y_L)}$$
$$+ \frac{(-2\tau_n - \beta c_2 \tau_n y_R)\kappa_3 + 2\beta^2 \sigma y_R \kappa_{4y} + 4\beta^2 \sigma \kappa_{5y}}{2\beta^2 \sigma \tau_n y_R(y_R + y_L)}$$
$$+ \frac{2\kappa_{7x}}{x_R x_L(y_R + y_L)} + \frac{4\kappa_8}{x_R x_L y_R(y_R + y_L)},$$

$$d_{31} = -\frac{\kappa_6}{(x_R + x_L)(y_R + y_L)} + \frac{2\kappa_{7x}}{x_L(x_R + x_L)(y_R + y_L)}$$
$$+ \frac{2\kappa_{7y}}{(x_R + x_L)y_L(y_R + y_L)} - \frac{4\kappa_8}{x_L(x_R + x_L)y_L(y_R + y_L)},$$

$$d_{32} = \frac{\kappa_6}{(x_R + x_L)(y_R + y_L)} + \frac{2\kappa_{7x}}{x_R(x_R + x_L)(y_R + y_L)}$$
$$- \frac{2\kappa_{7y}}{(x_R + x_L)y_L(y_R + y_L)} - \frac{4\kappa_8}{x_R(x_R + x_L)y_L(y_R + y_L)},$$

$$d_{33} = \frac{\kappa_6}{(x_R + x_L)(y_R + y_L)} - \frac{2\kappa_{7x}}{x_L(x_R + x_L)(y_R + y_L)}$$
$$+ \frac{2\kappa_{7y}}{(x_R + x_L)y_R(y_R + y_L)} - \frac{4\kappa_8}{x_L(x_R + x_L)y_R(y_R + y_L)},$$

$$d_{34} = -\frac{\kappa_6}{(x_R + x_L)(y_R + y_L)} - \frac{2\kappa_{7x}}{x_R(x_R + x_L)(y_R + y_L)}$$
$$- \frac{2\kappa_{7y}}{(x_R + x_L)y_R(y_R + y_L)} - \frac{4\kappa_8}{x_R(x_R + x_L)y_R(y_R + y_L)},$$

$$s_{1y} = -\frac{\kappa_{9y}}{y_R + y_L} + \frac{2\kappa_{10y}}{y_L(y_R + y_L)},$$

$$s_{1x} = -\frac{\kappa_{9x}}{x_R + x_L} + \frac{2\kappa_{10x}}{x_L(x_R + x_L)},$$

$$s_0 = \frac{3\kappa_3 - 4}{4\sigma} - \frac{2\kappa_{10x}}{x_R x_L} - \frac{2\kappa_{10y}}{y_R y_L},$$

$$s_{2x} = \frac{\kappa_{9x}}{x_R + x_L} + \frac{2\kappa_{10x}}{x_R(x_R + x_L)},$$

$$s_{2y} = \frac{\kappa_{9y}}{y_R + y_L} + \frac{2\kappa_{10y}}{y_R(y_R + y_L)},$$

$$M_1 = -\frac{\kappa_3}{\sigma}, M_2 = \frac{\kappa_3}{4\sigma}. \tag{16}$$

Through the prior deducing procedure, it can be seen that the truncation error of the Eq. (15) is $O(\tau_n^2 + \tau_n(x_R^2 - x_R x_L + x_L^2) + \tau_n(y_R^2 - y_R y_L + y_L^2) + (x_R^5 + x_L^5/x_R + x_L) + (y_R^5 + y_L^5/y_R + y_L))$. When $h = x_R = x_L = y_R = y_L$ and $\tau_n = h^2$, it owns spatial accuracy of fourth order and temporal accuracy of second order.

3. Adaptive Grid Structure

3.1. Adaptive Grid Structure in Time. The adaptation mesh technique in the temporal and the spatial direction is employed for solving the 2D problem of quenching type. Obviously, the 2D adaptive mesh algorithm can be derived from the 1D case. The arc-length monitor function of the temporal derivative function resulting from equal distribution principle is used to design the temporal and the spatial moving mesh algorithm, respectively. From Ref. [19, 20], a self-adaptive grid in the time direction is given as follows. A maximized ratio equation for computing the adaptive temporal interval τ_n is

$$\frac{\tau_n}{\tau_{n-1}} = \frac{\max\limits_{\substack{0<k<K \\ 0<j<J}} \sqrt{1 + \left[\left(\partial^2 u/\partial t^2\right)\left(x_k, y_j, t_{n-1/2}\right)\right]^2}}{\max\limits_{\substack{0<k<K \\ 0<j<J}} \sqrt{1 + \left[\left(\partial^2 u/\partial t^2\right)\left(x_k, y_j, t_{n+1/2}\right)\right]^2}}, n = 1, 2, \cdots \tag{17}$$

The standard uniform central difference formula is substituted for the $\partial^2 u/\partial t^2$ in Eq. (17). Of course, when the prior temporal step τ_{n-1} is given, the current temporal step τ_n can be calculated through Eq. (17).

3.2. Adaptive Grid Structure in Space. Let a spatial adaptation algorithm be deduced as follows. $W_x(x, t)$ is taken as the monitor function in x – direction and $W_y(y, t)$ is taken as the monitor function in y – direction.

$$W_x(x, t) = \sqrt{1 + \sum_{k=0}^{K} \left[\left(\partial^2 u/\partial t \partial x\right)(x, t)\right]^2}, 0 \le x \le 1, 0 \le t < T,$$

(18)

$$W_y(y, t) = \sqrt{1 + \sum_{j=0}^{J} \left[\left(\partial^2 u/\partial t \partial y\right)(y, t)\right]^2}, 0 \le y \le 1, 0 \le t < T.$$

(19)

$\{\xi_k(x_k, t)\}_{k=0}^{K}$ and $\{\zeta_j(y_j, t)\}_{j=0}^{J}$ point to the set of 2D original spatial mesh points in x − direction and y − direction. The 2D computational area is transformed as $\{x_k(\xi_k, t)\}_{k=0}^{K}$ in x − direction and $\{y_j(\zeta_j, t)\}_{j=0}^{J}$ in y − direction through mesh movement. The continuous function $W_x(x, t) > 0$ and $W_y(y, t) > 0$ in the definition area $(x, y) \in (0, 1) \times (0, 1)$ equally distributes over the 2D mesh refreshed. In fact, the 1D adaptive mesh algorithm individually carries out in each spatial direction. According to [19, 20], we can get the semi-implicit scheme in x − direction

$$W_x\left(x_{k+1/2}^{(m)}, t_n\right)\left(x_{k+1}^{(m+1)} - x_k^{(m+1)}\right)$$
$$- W_x\left(x_{k-1/2}^{(m)}, t_n\right)\left(x_k^{(m+1)} - x_{k-1}^{(m+1)}\right)$$

(20)

$$= 0, k = 1, 2, \cdots, K - 1, n \ge 0.$$

Similarly, we can get the semi-implicit scheme in y − direction

$$W_y\left(y_{j+1/2}^{(m)}, t_n\right)\left(y_{j+1}^{(m+1)} - y_j^{(m+1)}\right)$$
$$- W_y\left(y_{j-1/2}^{(m)}, t_n\right)\left(y_j^{(m+1)} - y_{j-1}^{(m+1)}\right)$$

(21)

$$= 0, j = 1, 2, \cdots, J - 1, n \ge 0.$$

3.3. Iterative Adaption Algorithm. This paragraph shows the iterative process of the presented method in the paper.

Step 1. Depending on the spatial mesh $\{x_k^{(m)}\}_{k=0}^{K}$, $\{y_j^{(m)}\}_{j=0}^{J}$ at the nth time layer, we can obtain the corresponding monitor functions $W_x(x, t)$ and $W_y(y, t)$ via Eqs. (18) and (19).

Step 2. The point set $\{x_k^{(m+1)}\}_{k=0}^{K}$ refreshed is extracted from the prior grid $\{x_k^{(m)}\}_{k=0}^{K}$ via Eq. (20) whereas $\{y_j^{(m+1)}\}_{j=0}^{J}$ refreshed is extracted from $\{y_j^{(m)}\}_{j=0}^{J}$ by Eq. (21). We use the new point sets to get the replacement for the old point sets iteratively once $\sum_{k=1}^{K-1}\|x_k^{(m+1)} - x_k^{(m)}\| < er$, $\sum_{j=1}^{J-1}\|y_j^{(m+1)} - y_j^{(m)}\| < er$, which er takes 10^{-5}. The last value of $m + 1$ takes M_n.

Step 3. By virtue of the last grid point sets $\{x_k^{(M_n)}\}_{k=0}^{K}$, $\{y_j^{(M_n)}\}_{j=0}^{J}$, and area ratio algorithm, the solutions in the n

th time line $\{u_{k,j}^n\}_{k=1,j=1}^{K-1,J-1}$ are all estimated. Combining with τ_n obtained from Eq. (17), $\{u_{k,j}^{n+1}\}_{k=1,j=1}^{K-1,J-1}$ in the $n + 1$th time line can be calculated by Eq. (15).

Step 4. Repeat steps from the first to the third till quenching occurs, or the solution converges to a steady solution.

4. Simulation Demonstration

4.1. Numerical Case. This is a common numerical sample utilized to evaluate the performance of Eq. (15) measure by Eq. (22)

$$pu_t = u_{xx} + u_{yy} - pu_x - pu_y, (x, y) \in [0, 1] \times [0, 1], t \ge 0,$$

(22)

$$u(x, y, t) = \frac{e^{px} - 1}{e^p - 1} + \frac{e^{py} - 1}{e^p - 1}$$
$$+ \sum_{q=1}^{\infty} \frac{(-1)^q q\pi}{(q\pi)^2 + p^2/4} e^{p(x-1)/2 + p(y-1)/2} \sin$$

(23)

$$\cdot (q\pi x + q\pi y)e^{-\left[(q\pi)^2/p + p/4\right]t}.$$

In the paper, $T = 0.5, \tau_n = 0.01, p = 100$. The initial and boundary values can be computed through the exact solution. The tested results display in Table 1, in which there are four criteria containing Max. error, Aver. error, CPU time, and Conv. rate. Max. error means the maximal absolute error between analysis solution and difference solution; Aver. error means the average absolute error; CPU time means the running time of system; Conv. rate means convergence rate between the two interfacing mesh numbers. The nonuniform mesh follows the rule: $\{k/K + (\lambda_x/\pi) \sin (\pi k/K)\}_{k=0}^{K}$ in x − direction and $\{j/J + (\lambda_y/\pi) \sin (\pi j/J)\}_{j=0}^{J}$ in y − direction, where K and J point to intervals of spatial direction and $K = J$, whereas λ_x and λ_y mean telescopic transformation coefficient and $\lambda_x = \lambda_y$. There exist six difference schemes that are compared on another for the example in Table 1, which are the schemes in Ref. [26] on the uniform and the nonuniform grid, the schemes in Ref. [27] on the uniform and the nonuniform grid, and the proposed schemes on the uniform and the nonuniform grid. The schemes in Ref. [27] and the proposed schemes all chose the five spatial intervals 16, 32, 64, 128, 256, and $\lambda_x = \lambda_y = 0.7$ and the four aforementioned criteria. Only the schemes in Ref. [26] choose the five spatial intervals 16, 32, 64, 128, and $\lambda_x = \lambda_y = 0.4$ and the three aforementioned criteria with the exception of Aver. error.

With regard to Max. error and Aver. error, the schemes on the uniform grid are inferior to the schemes on the nonuniform grid; the proposed schemes are superior to the other schemes, and the schemes (nonuniform) in Ref. [27] are superior to the scheme (nonuniform) in Ref. [26], and the tendency becomes more obviously as $K(J)$ rises. When $K(J)$ is 128, the maximal absolute error of the scheme in Ref. [27] (uniform) is 3.1469×10^{-4}, and the maximal absolute error of the scheme in Ref. [27] (nonuniform) is 9.3004×10^{-7}; the maximal absolute error of the scheme in Ref. [26]

TABLE 1: The parameter values for common example.

Schemes	$K(J)$	Max. error	Aver. error	CPU time	Conv. rate
The scheme in Ref. [26] (uniform)	16	2.59×10^{-1}	—	1000	—
	32	5.65×10^{-2}	—	1344	2.30
	64	5.50×10^{-3}	—	6766	3.44
	128	3.15×10^{-4}		61328	4.17
The scheme in Ref. [26] (nonuniform)	16	1.12×10^{-1}	—	844	—
	32	1.22×10^{-2}	—	1625	3.34
	64	6.84×10^{-4}	—	11188	4.25
	128	4.42×10^{-5}	—	135344	4.00
The scheme in Ref. [27] (uniform)	16	2.4859×10^{-1}	1.7858×10^{-2}	47	—
	32	5.7032×10^{-2}	1.9148×10^{-3}	172	5.0033
	64	5.5382×10^{-3}	1.4565×10^{-4}	702	3.7166
	128	3.1469×10^{-4}	9.6850×10^{-6}	2948	3.9106
	256	1.9710×10^{-5}	6.1742×10^{-7}	11794	3.9714
The scheme in Ref. [27] (nonuniform)	16	8.1898×10^{-3}	8.7725×10^{-4}	358	—
	32	2.9724×10^{-4}	2.9996×10^{-5}	2855	7.9861
	64	1.5573×10^{-5}	1.6521×10^{-6}	14914	4.1824
	128	9.3004×10^{-7}	1.0224×10^{-7}	35006	4.1964
	256	1.3364×10^{-7}	6.4492×10^{-9}	165969	4.7029
The proposed scheme (uniform)	16	2.5865×10^{-1}	1.7571×10^{-2}	78	—
	32	5.6511×10^{-2}	1.9107×10^{-3}	297	4.9902
	64	5.5041×10^{-3}	1.4562×10^{-4}	1217	3.7138
	128	3.1447×10^{-4}	9.6804×10^{-6}	5148	3.9110
	256	1.9357×10^{-5}	5.9061×10^{-7}	20951	4.0348
The proposed scheme (nonuniform)	16	8.1405×10^{-3}	8.7581×10^{-4}	421	—
	32	2.9716×10^{-4}	2.9989×10^{-5}	1857	7.9849
	64	1.5491×10^{-5}	1.6490×10^{-6}	6911	4.1847
	128	6.9033×10^{-7}	8.9949×10^{-8}	24585	4.1964
	256	4.1212×10^{-8}	3.4536×10^{-9}	131243	4.7029

(uniform) is 3.15×10^{-4}, and the maximal absolute error of the scheme in Ref. [26] (nonuniform) is 4.42×10^{-5}; the maximal absolute error of the proposed scheme (uniform) is 3.1447×10^{-4}, and the maximal absolute error of the proposed scheme (nonuniform) is 6.9033×10^{-7}. When $K(J)$ is 256, the average error of the scheme in Ref. [27] (uniform) is 6.1742×10^{-7}, and the average error of the scheme in Ref. [27] (nonuniform) is 6.4492×10^{-9}; the average error of the proposed scheme (uniform) is 5.9061×10^{-7}, and the average error of the proposed scheme (nonuniform) is 3.4536×10^{-9}. In terms of CPU time, the scheme (nonuniform) in Ref. [27] spends the most time among the schemes when $K(J)$ is 32, 64, 128, and 256, and the tendency becomes more obviously as $K(J)$ rises; the schemes in Ref. [26] spend much more time than the proposed schemes do. Typically, the running time of the schemes on the uniform grid is less than that of the schemes on the nonuniform grid. It just means that the latter complies with a time-for-space rule, which refers to it may improve the spatial accuracy of an algorithm by adding its running time.

4.2. Quenching Case without Convection Term. When $c_1(x, y) = 0$ and $c_2(x, y) = 0$, with the initial and boundary conditions Eqs. (6) and (7), the original Eq. (5) can be described as

$$
\begin{aligned}
\left(\alpha^2 x^2 + \beta^2 y^2\right)^{q/2} u_t &= \frac{1}{\alpha^2} u_{xx} + \frac{1}{\beta^2} u_{yy} \\
&\quad + \frac{1}{(1-u)^\theta}, (x, y) \in (0, 1) \\
&\quad \times (0, 1), t \in (0, T).
\end{aligned} \tag{24}
$$

TABLE 2: Quenching performances of different schemes for $q = 0$, $a = \beta = \sqrt{10}$, and $\theta = 1$ without convection term.

Schemes	$x_{\max}$	$y_{\max}$	$T_{\max}$	max u	max u_t
The proposed scheme	0.500	0.500	0.5990174307488624	0.9901182463562488	83.20947696438735
The scheme in [19]	—	—	0.58712499993751	0.990432	148.887767
The scheme in [20]	0.500	0.500	0.587554	0.999263	1249.917563

For the situation of $c_1(x, y) = 0$ and $c_2(x, y) = 0$, we take advantage of Eq. (15) to approximate Eq. (24) and gain quenching case without convection term. We set the three parameters $q = 0$, $a = \beta = \sqrt{10}$, and $\theta = 1$ to the case which had been illustrated in Refs [19, 20]. In this case, the initial temporal step is configured as $\tau_0 = 4.166677 \times 10^{-5}$, and the initial space step is configured as $h_0 = 1/90$.

Table 2 offers quenching performances of the three different schemes, which are from Refs [19, 20] besides the proposed method on adaptive mesh, for $q = 0$, $a = \beta = \sqrt{10}$, and $\theta = 1$ without convection term. The criteria in Table 2 are explained as follows. $(x_{\max}, y_{\max})$ refers to the point of quenching location, $T_{\max}$ refers to the quenching time, max u refers to the maximum temperature value immediately before quenching happens, and max u_t refers to the maximum variation of temperature with respect to time immediately before quenching happens. For the three schemes, their quenching locations are all $(0.5, 0.5)$. There are subtle differences among the three schemes for quenching time and max u. $T_{\max}$ of the proposed scheme is 0.5990174307488624, and max u of the proposed scheme is 0.9901182463562488. But there are greater differences among the three schemes for max u_t. max u_t of the proposed scheme is 83.20947696438735 while those of the schemes in Refs [19, 20] are 148.887767 and 1249.917563. There is no effect of the differences on quenching research. Figure 1 offers the three-dimensional scenes of u and u_t with regard to spatial variables x, y when the time t is 0.5990174307488624, respectively. From the two 3D surfaces at the time $T_{\max} = 0.5990174307488624$ that is immediately before quenching occurs, it is found that $u \longrightarrow 1^-$ and $u_t \longrightarrow 84^-$ at the quenching location $(x_{\max}, y_{\max}) = (0.5, 0.5)$ and the quenching time $T_{\max} = 0.5990174307488624$.

4.3. Quenching Case with Convection Term $b/(1 + \alpha x + \beta y)$. We will investigate what role degeneration parameter q, convection parameter b, and combustion chamber size $\alpha(\beta)$ in Eqs. (5)–(7) play during the quenching process and enumerate the representative Case 5.0 to show special quenching features when $c_1(x, y) = b_x/(1 + \alpha x + \beta y)$ and $c_2(x, y) = b_y/(1 + \alpha x + \beta y)$, where b_x and b_y take the constants and convection parameter $b = b_x = b_y$. When singularity parameter θ is larger than 1, the quenching situation is complex. Therefore, we only consider quenching cases of $\theta = 1$. In numerical samples, b_x and b_y range from -200 to 200; α^2 range from 15 to 300000. These are the same to Section 4.4. To better illustrate the problems, we choose some representative data from lots of tests to discuss quenching phenomena in the next paragraphs. For the convection model $b/(1 + \alpha x + \beta y)$, we set $h_0 = 1/70$ as the initial $x - (y-)$ step and $\tau_0 = 0.0008$ as the initial t-step.

Tables 3–6 offer some typical quenching cases to demonstrate the relationship between the three groups of parameters and quenching phenomena. Case 5.0 recorded as a reference in Table 3, i.e., $q = 1$, $b_x = b_y = 3$, $\alpha = \beta = 15$, is compared with other cases in Tables 3–5. Table 6 displays the specific quenching data of Case 5.0. Figures 1–3 show the quenching statuses of Case 5.0 relative to u, u_t, x, y, and t.

Except Case 5.0, there are ten quenching cases chosen in Table 3. The ten items list as follows: Case 5.1.1 is $q = 0.1$, $b_x = b_y = 3$, $\alpha = \beta = 15$; Case 5.1.2 is $q = 0.2$, $b_x = b_y = 3$, $\alpha = \beta = 15$; Case 5.1.3 is $q = 0.4$, $b_x = b_y = 3$, $\alpha = \beta = 15$; Case 5.1.4 is $q = 0.6$, $b_x = b_y = 3$, $\alpha = \beta = 15$; Case 5.1.5 is $q = 0.7$, $b_x = b_y = 3$, $\alpha = \beta = 15$; Case 5.1.6 is $q = 0.9$, $b_x = b_y = 3$, $\alpha = \beta = 15$; Case1.1.7 is $q = 1.1$, $b_x = b_y = 3$, $\alpha = \beta = 15$; Case1.1.8 is $q = 1.2$, $b_x = b_y = 3$, $\alpha = \beta = 15$; Case 5.1.9 is $q = 1.3$, $b_x = b_y = 3$, $\alpha = \beta = 15$; Case 5.1.10 is $q = 1.4$, $b_x = b_y = 3$, $\alpha = \beta = 15$. Although the program may run when $q \geq 1.5$, it is hard to form quenching behaviors. If q belongs to the definition domain $[0.1, 1.4]$, the quenching phenomena will occur. From serial numerical cases, we can easily see the performances of quenching location and time. The quenching location $(x_{\max}, y_{\max})$ declines as q evolves and finally converges to $(0.04285714285714286, 0.04285714285714286)$. There is an intermediate point $q = 0.9$ dividing the definition domain as $[0.1, 0.9]$ and $[1.0, 1.4]$. The quenching location $x_{\max}$ and $y_{\max}$ do decline as q evolves in the first subdomain and converge to $(0.04285714285714286, 0.04285714285714286)$ in the second subdomain. The quenching time $T_{\max}$ reaches the maximum 9.686902288384093 when $q = 1.4$. $T_{\max}$ and q are in positive proportion when q in $[0.1, 1.4]$.

We choose ten items written in Table 4 to display the quenching characteristics related to the parameters b_x and b_y. Case 5.2.1 is $q = 1$, $b_x = b_y = -5$, $\alpha = \beta = 15$; Case 5.2.2 is $q = 1$, $b_x = b_y = -3$, $\alpha = \beta = 15$; Case 5.2.3 is $q = 1$, $b_x = b_y = 0$, $\alpha = \beta = 15$; Case 5.2.4 is $q = 1$, $b_x = b_y = 2$, $\alpha = \beta = 15$; Case 5.2.5 is $q = 1$, $b_x = b_y = 4$, $\alpha = \beta = 15$; Case 5.2.6 is $q = 1$, $b_x = b_y = 5$, $\alpha = \beta = 15$; Case 5.2.7 is $q = 1$, $b_x = b_y = 6$, $\alpha = \beta = 15$; Case 5.2.8 is $q = 1$, $b_x = b_y = 8$, $\alpha = \beta = 15$; Case 5.2.9 is $q = 1$, $b_x = b_y = 9$, $\alpha = \beta = 15$; Case 5.2.10 is $q = 1$, $b_x = b_y = 10$, $\alpha = \beta = 15$; b_x and b_y in Eq. (5) are theoretically equivalent, i.e., $b = b_x = b_y$. A valid scope of b is $[-5, 10]$ for these cases. Because quenching occurs fastest when b takes 4, $b = 4$ is thought as a special point for quenching time. Quenching time is inversely proportional to b when $b \in [-5, 4]$ and positively proportional to b when $b \in [4, 10]$. Quenching location $(x_{\max}, y_{\max})$ rises as b increases when $b \in [-5, 5]$ and takes $(0.02857142857142857, 0.02857142857142857)$ when $b \geq 6$.
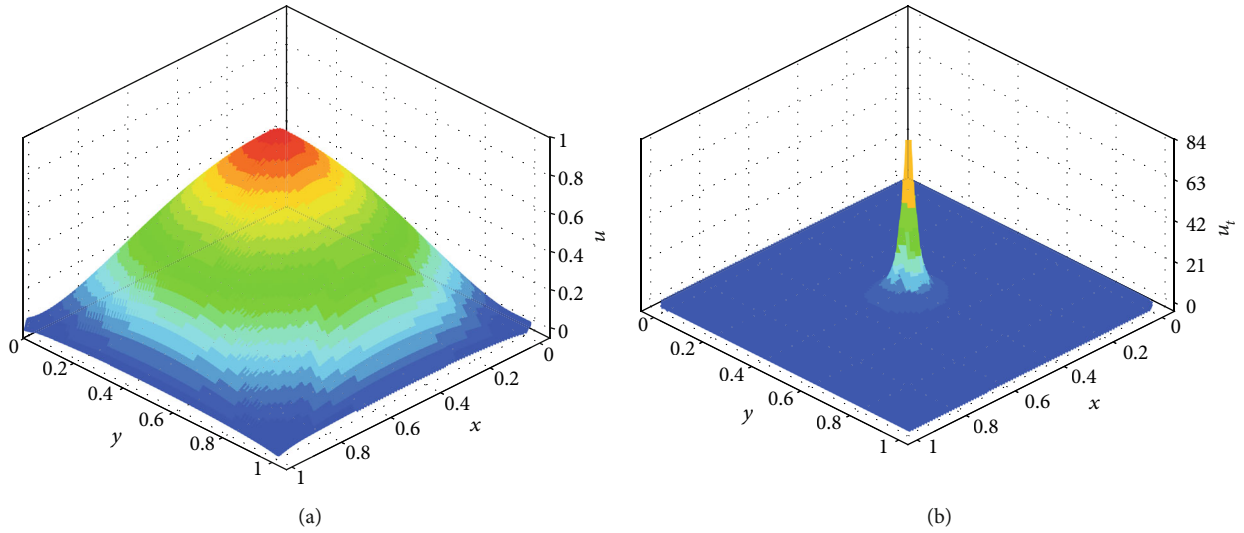
<center>(a)</center>

<center>(b)</center>

FIGURE 1: (a) The 3D plots of u immediately before quenching occurs, and (b) the 3D plots of u_t immediately before quenching occurs. The parameters are $q = 0$, $a = \beta = \sqrt{10}$, and $\theta = 1$ without convection term.

<center>TABLE 3: Quenching data of q based on convection term $b/(1 + \alpha x + \beta y)$.</center>

Case name	$x_{\max}$	$y_{\max}$	$T_{\max}$	max u	max u_t
Case 5.0	0.04285714285714286	0.04285714285714286	3.428404873627137	0.9920620807720361	125.6265973017968
Case 5.1.1	0. 1	0.1	0.6470842629145379	0.9933649818060033	136.4723853886283
Case 5.1.2	0.08571428571428572	0.08571428571428572	0.7824847046607435	0.9903819718639215	87.67058865539519
Case 5.1.3	0.07142857142857143	0.07142857142857143	1.109942679446164	0.9908479463229512	86.47536110256003
Case 5.1.4	0.05714285714285714	0.05714285714285714	1.572860422734615	0.9902786764164395	83.87879039070892
Case 5.1.5	0.05714285714285714	0.05714285714285714	1.88098095097722	0.9920140466370957	101.1277413288689
Case 5.1.6	0.05714285714285714	0.05714285714285714	2.771928557465351	0.9920059842963465	96.8866420271182
Case 5.1.7	0.04285714285714286	0.04285714285714286	4.293156056984269	0.9908925785572684	107.7822215514385
Case 5.1.8	0.04285714285714286	0.04285714285714286	5.485318052886954	0.9920945867539992	126.7837317275917
Case 5.1.9	0.04285714285714286	0.04285714285714286	7.182200512059787	0.9903718441627313	102.1421834048094
Case 5.1.10	0.04285714285714286	0.04285714285714286	9.686902288384093	0.992048580687276	127.8241083054763

<center>TABLE 4: Quenching data of b_x and b_y based on convection term $b/(1 + \alpha x + \beta y)$.</center>

Case name	$x_{\max}$	$y_{\max}$	$T_{\max}$	max u	max u_t
Case 5.2.1	0.1714285714285714	0.1714285714285714	8.379050080786115	0.990231496274097	27.01166111192879
Case 5.2.2	0.1285714285714286	0.1285714285714286	6.144661979620801	0.9902084486956095	35.54184621151833
Case 5.2.3	0.08571428571428572	0.08571428571428572	4.133262574622704	0.9902265728041954	52.5010571873496
Case 5.2.4	0.05714285714285714	0.05714285714285714	3.540661768514728	0.9901040464540505	75.11254034765163
Case 5.2.5	0.04285714285714286	0.04285714285714286	3.389328541055185	0.992283726259128	128.3227508596781
Case 5.2.6	0.04285714285714286	0.04285714285714286	3.449401822644199	0.9910523423231372	108.73967781816
Case 5.2.7	0.02857142857142857	0.02857142857142857	3.578376058086737	0.990585829058986	147.5334079485446
Case 5.2.8	0.02857142857142857	0.02857142857142857	4.018879993939997	0.9940259443236479	246.3627497716133
Case 5.2.9	0.02857142857142857	0.02857142857142857	4.341185345099308	0.9904731250696808	143.5523827878386
Case 5.2.10	0.02857142857142857	0.02857142857142857	4.731222306735877	0.9969319295625433	506.9119438251631

Table 5 offers seventeen referencing cases. The first ten items are Case 5.3.1 is $q = 1$, $b_x = b_y = 3$, $\alpha/\beta = 1$, $\alpha^2 = 15$; Case 5.3.2 is $q = 1$, $b_x = b_y = 3$, $\alpha/\beta = 1$, $\alpha^2 = 1227$; Case 5.3.3 is $q = 1$, $b_x = b_y = 3$, $\alpha/\beta = 1$, $\alpha^2 = 1228$; Case 5.3.4 is $q = 1$, b_x $= b_y = 3$, $\alpha/\beta = 1$, $\alpha^2 = 1229$; Case 5.3.5 is $q = 1$, $b_x = b_y = 3$, $\alpha/\beta = 1$, $\alpha^2 = 2900$; Case 5.3.6 is $q = 1$, $b_x = b_y = 3$, $\alpha/\beta = 1$, $\alpha^2 = 2999$; Case 5.3.7 is $q = 1$, $b_x = b_y = 3$, $\alpha/\beta = 1$, $\alpha^2 = 3000$; Case 5.3.8 is $q = 1$, $b_x = b_y = 3$, $\alpha/\beta = 1$, $\alpha^2 = 8 \times 10^4$; Case

TABLE 5: Quenching data of α and β based on convection term $b/(1 + \alpha x + \beta y)$.

Case name	x_{max}	y_{max}	T_{max}	max u	max u_t
Case 5.3.1	0.20	0.20	3.621624575204209	0.991718707508642	86.83309533401254
Case 5.3.2	0.02857142857142857	0.02857142857142857	3.609153368630949	0.9907185674353032	73.0239115821952
Case 5.3.3	0.01428571428571429	0.01428571428571429	3.609390601249229	0.9912265622789864	150.6673183543721
Case 5.3.4	0.01428571428571429	0.01428571428571429	3.609274948219342	0.9919688690187356	165.4554013002607
Case 5.3.5	0.01428571428571429	0.01428571428571429	3.376127343223672	0.9902039498799047	90.20671661807094
Case 5.3.6	0.01428571428571429	0.01428571428571429	3.378639256536471	0.9927000295904764	120.3354981361145
Case 5.3.7	0.01428571428571429	0.01428571428571429	3.378668197610872	0.9923048003313988	113.9606848017258
Case 5.3.8	0.01428571428571429	0.01428571428571429	23.38176644203467	0.9900781386538231	17.60457567575462
Case 5.3.9	0.01428571428571429	0.01428571428571429	31.0931917834407	0.9900013538386812	14.90527975955028
Case 5.3.10	0.01428571428571429	0.01428571428571429	39.49651984658089	0.990003317828528	13.07949247781412

TABLE 6: The maximal values and locations of u and u_t for $q = 1$, $b_x = b_y = 3$, $\alpha = \beta = 15$ based on convection term $b/(1 + \alpha x + \beta y)$.

| t	x	y	$\max_{x,y} u$	$\max_{x,y}(u_t)$
3.428290495431297	0.04285714285714286	0.04285714285714286	0.983134449815426	53.0703838235108
3.428342645817735	0.04285714285714286	0.04285714285714286	0.863372971410449	68.08063220416238
3.428379787989620	0.04285714285714286	0.04285714285714286	0.9893206357439858	90.30503152559813
3.428404873627137	0.04285714285714286	0.04285714285714286	0.9920620807720361	125.6265973017968
3.428420657560073	—	—	17.07446290189856	$1.200141619871376 \times 10^9$
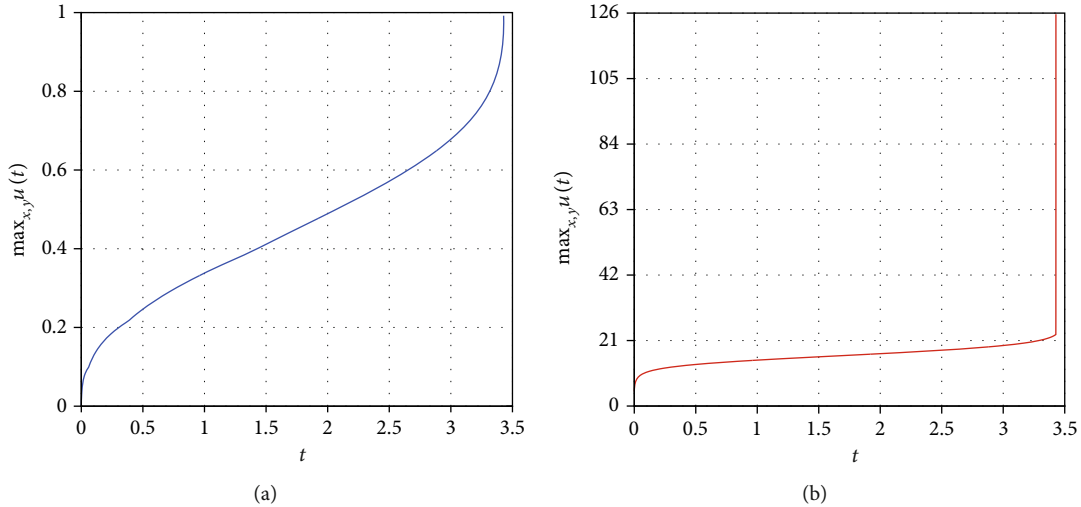
FIGURE 2: The graphs of solution u and u_t: (a) $\max_{x,y} u$ as t increases, and (b) $\max_{x,y}(u_t)$ as t increases from the initial moment to the occurrence of quenching behavior with the parameters $q = 1$, $b_x = b_y = 3$, $\alpha = \beta = 15$ based on convection term $b/(1 + \alpha x + \beta y)$.

5.3.9 is $q = 1$, $b_x = b_y = 3$, $\alpha/\beta = 1$, $\alpha^2 = 1.1 \times 10^5$; Case 5.3.10 is $q = 1$, $b_x = b_y = 3$, $\alpha/\beta = 1$, $\alpha^2 = 1.43 \times 10^5$. We configure $15 \le \alpha^2 \le 1.43 \times 10^5$ and $\alpha/\beta = 1$ for the prior ten items. Experiments show even if α^2 reaches 10^5, quenching phenomena still happen. Furthermore, if α^2 falls in the interval $[15, 1.43 \times 10^5]$, then quenching phenomena will occur normally, and quenching location x_{max} and y_{max} do not decrease monotonously as α^2 declines. When α^2 lies in the area of $[1228, 1.43 \times 10^5]$, (x_{max}, y_{max}) always keeps $(0.01428571428571429, 0.01428571428571429)$. In terms of quenching time, there is no obvious linear relationship

between T_{max} and α^2 in a small range of the definition field of α^2. If the measurement scale is enlarged in the domain of α^2, especially when α^2 reaches 2900, T_{max} will rise with the increase of α^2, i.e., T_{max} is 3.376127343223672 when α^2 is 2900 and T_{max} is 39.49651984658089 when α^2 is 1.43×10^5.

We take Case 5.0 to demonstrate specific quenching phenomena. In this case, quenching occurs at $T_5* = 3.428404873627137$, $x_5* = 0.04285714285714286$, and $y_5 * = 0.04285714285714286$ with the parameters $q = 1$, $b_x = b_y = 3$, $\alpha = \beta = 15$. The next context declares more details about quenching. Let us observe the performances of the
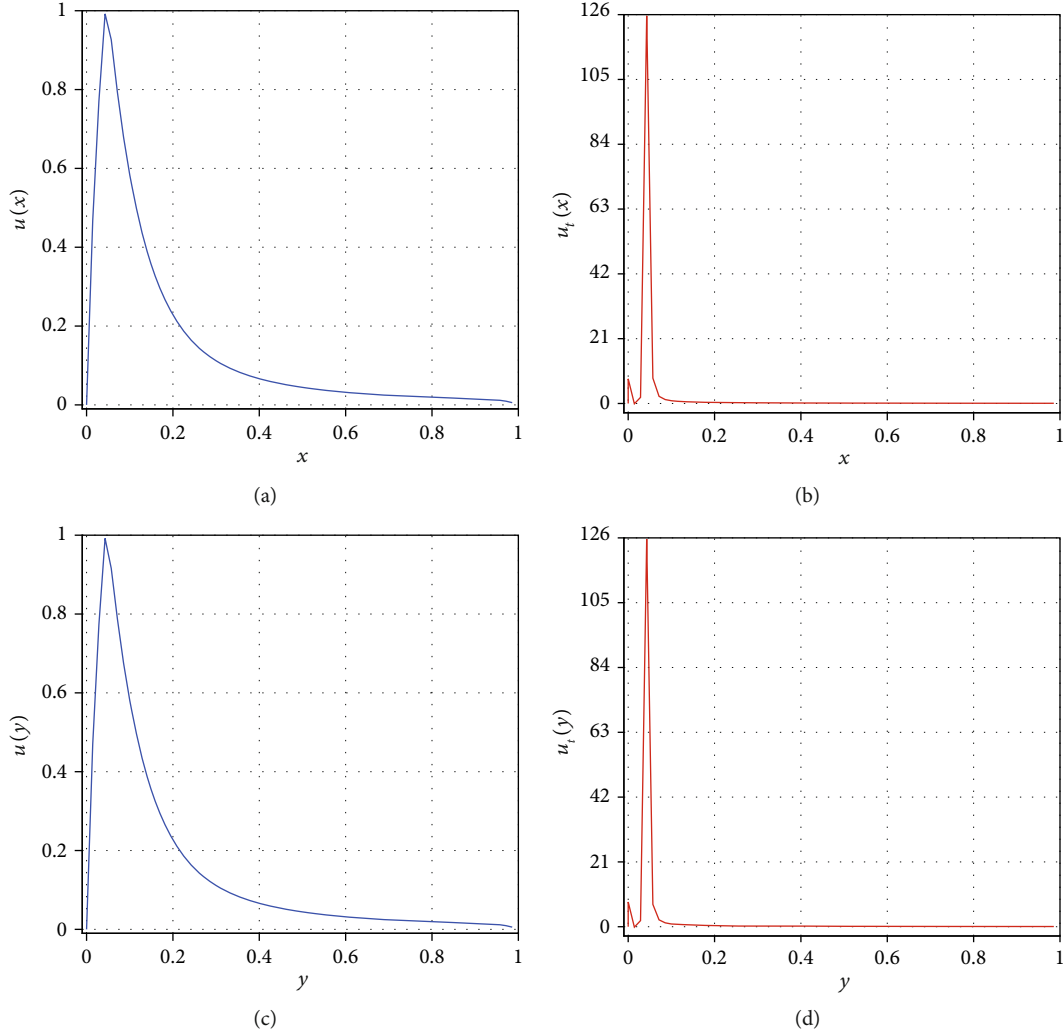
(a)

(b)

(c)

(d)

FIGURE 3: The graphs of (a) u as x increases, (b) u_t as x increases, (c) u as y increases, and (d) u_t as y increases when t is $T_5 *$ for convection term $b/(1 + \alpha x + \beta y)$.

solution u, the derivative function u_t, and their time and space locations of five stages relative to quenching for Case 5.0, which show in Table 6 and Figures 2–4. The first four items reflect the four states before quenching occurs in Table 6. The last item represents the quenching state in which u is more than 1 and reaches 17.07446290189856, u_t blows up and reaches $1.200141619871376 \times 10^9$, the position of $\max_{x,y} u$ is $(0.5336298640841476 \times 10^{-5}, 0.2902651144597507)$, and the position of $\max_{x,y}(u_t)$ is $(0.5702149685882448 \times 10^{-4}, 0.5677032305886261 \times 10^{-4})$ when $t = 3.428420657560073$. Figures 2(a) and 2(b) denote the profiles of both solution u and derivative function u_t. In the aforementioned figures, the maximum values of u and u_t grow from 0 to $T_5 *$. As soon as time variable t arrives at quenching spot $(x_5 *, y_5 *)$ and quenching time $T_5 *$, we have $\max u = 0.99206208077203618$ and $\max (u_t) = 125.6265973017968$. By locating the quenching time $T_5 *$, we can draw the plots of $\max_{x,y} u(t)$ and $\max_{x,y} u_t(t)$. Figures 3(a)–3(d) depict the function relationships between u and x, between u_t and x, between u and y, and between u_t and y, respectively, when t is $T_5 *$. Owing to the identity of x

and y in the original equation, Figures 3(a) and 3(c) have the same shape, and Figures 3(b) and 3(d) have the same shape.

Figure 4 depicts curve of the adaptive temporal steps as the time variable progresses and graphs of the adaptive spatial steps changing as the space variables change. Figures 4(a) and 4(b) portray the distributions of spatial steps. The plots in Figure 4(a) are similar to those in Figure 4(b), but there are some subtle differences in their specific data. The blue curve depicts the tendency of spatial steps varying before quenching occurs, which underlines $x_5 *(y_5 *)$. The green line refers to spatial step distribution of uniform mesh with nonadaption, which is extracted from the initial temporal layer. Mesh adaptation is stimulated at the position of red square sign, and τ_n becomes gradually smaller and falls rapidly toward its floor when $t \longrightarrow T_5 *$ in Figure 4(c). The red square mark represents the moment $t = 3.425399077950409$ and the temporal step $\tau_n = 5.990779506555022 \times 10^{-4}$ when the process approximates to quenching time. The time adaption is triggered before the moment $T_5 *$ and lasts through the rest course of calculation. So this quenching phenomenon is caught with the features of $\max_{x,y} u \longrightarrow 1^-$ and $\max_{x,y}(u_t) \longrightarrow 126^-$ as t reaches $T_5 *$.
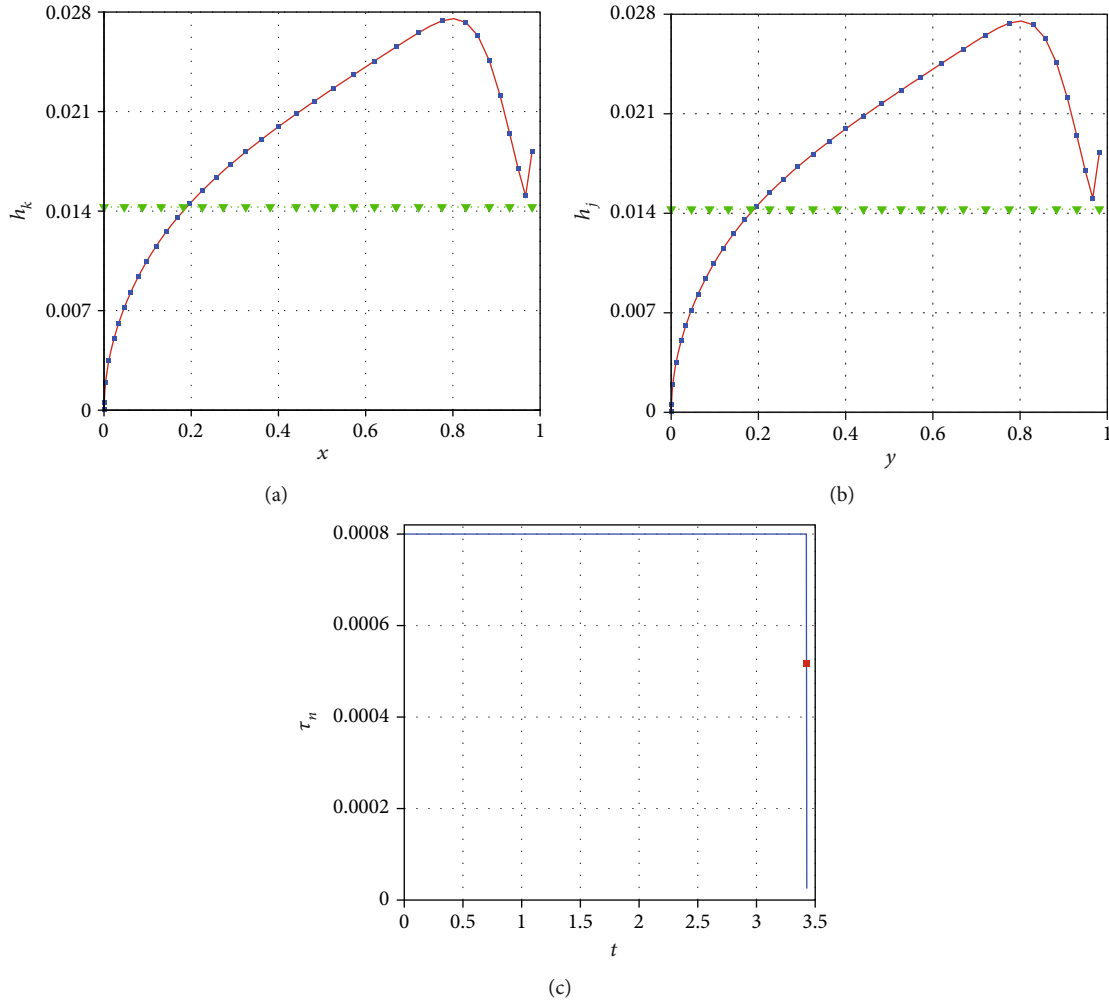
(a)

(b)

(c)

FIGURE 4: (a) The variation of spatial step h_k as x processes; (b) the variation of spatial step h_j as y processes; (c) the curve of the temporal steps τ_n as time t increases with the parameters $q = 1$, $b_x = b_y = 3$, $\alpha = \beta = 15$ based on convection term $b/(1 + \alpha x + \beta y)$.

There are three groups of 3D profiles of the solutions and their temporal derivatives in Figure 5. Figures 5(a) and 5(b) denote the two three-dimensional plots of u and u_t when $t = 0.40$, respectively. Figures 5(c) and 5(d) denote the two three-dimensional plots of u and u_t when $t = 3.428342645817735$, respectively. Figures 5(e) and 5(f) denote the two three-dimensional plots of u and u_t when $t = T_5 *$, respectively. Thought the 3D plots, we can get richer information. The first group is the three-dimensional views from both u and u_t at the first 500th temporal layers in the excursion, in which $\max_{x,y} u \longrightarrow 0.2215$ and $\max_{x,y}(u_t) \longrightarrow 12.9459$ when $t = 0.40$. The second group is the three-dimensional views from both u and u_t including the penultimate temporal steps before $T_5 *$, in which $\max_{x,y} u \longrightarrow 0.9863$ and $\max_{x,y}(u_t) \longrightarrow 68.0806$ when $t = 3.428342645817735$. The third group is the three-dimensional views from both u and u_t immediately before quenching happens, in which $\max_{x,y} u \longrightarrow 0.9921$ and $\max_{x,y}(u_t) \longrightarrow 125.6266$ when $t = 3.428404873627137$. During the temporal layers' moving forward, the solution u changes smoothly and then almost arrives at the peak value while t approximates to $T_5 *$. Its peak is the maximal value but before

quenching time and location. There is some subtle perturbation at the initial temporal axis of the left boundary for the change rate of the solution. Afterward, the temporal derivative varies smoothly, and their maximums of each time axis increase steadily. While t approaches to the quenching time $T_5 *$, the maximum u_t also increases rapidly and infinitely and then blows up at the next time layer of quenching time.

4.4. Quenching Example with Convection Term $b/(\alpha x + \beta y)$. Similarly, we need to only consider $\theta = 1.0$ and conduct a series of simulation experiments to investigate the 2D quenching regularity for the convection term $b/(\alpha x + \beta y)$ which is related to the three groups of elements: q and b_x and b_y, α, and β and exemplify the quenching behaviors of the representative Case 6.0. The convection term $b/(\alpha x + \beta y)$ should written as $c_1(x, y) = b_x/(\alpha x + \beta y)$ and $c_2(x, y) = b_y/(\alpha x + \beta y)$, where b_x and b_y take the constants and convection parameter $b = b_x = b_y$. For Case 6.0, the initial $x -$ step is $h_0 = 1/80$, and the initial $t -$ step is $\tau_0 = 0.001$. We choose some representative data to record in Tables 7–10 from the simulation results. Case 6.0 is regarded as the reference standard
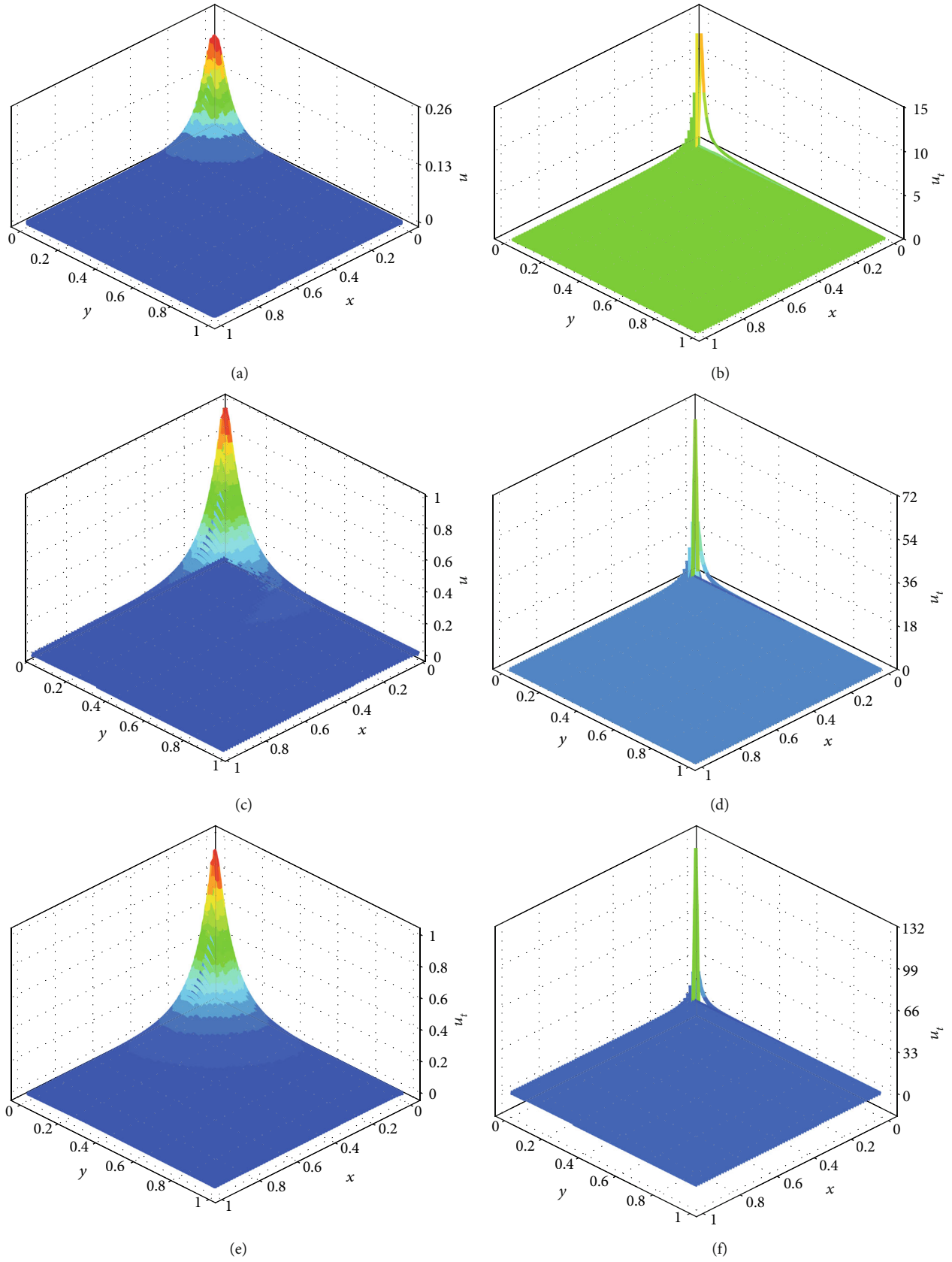
FIGURE 5: (a) The 3D plot of u when $t = 0.40$; (b) the 3D plot of u_t when $t = 0.40$; (c) the 3D plot of u when $t = 3.428342645817735$; (d) the 3D plot of u_t when $t = 3.428342645817735$; (e) the 3D plot of u when $t = T_5 *$; (f) the 3D plot of u_t when $t = T_5 *$. All is for Case 5.0.

TABLE 7: Quenching data of q based on convection term $b/(\alpha x + \beta y)$.

Case name	x_{max}	y_{max}	T_{max}	max u	max u_t
Case 6.0	0.0125	0.0125	4.020449234557191	0.981186659892471	31.34049546140411
Case 6.1.1	0.025	0.0375	0.4893400471790108	0.9815547233986595	53.96815295250957
Case 6.1.2	0.025	0.025	1.40546552826671	0.9810673165994175	30.97740120847389
Case 6.1.3	0.025	0.0125	1.806856006612364	0.9835285046535343	34.84710326333095
Case 6.1.4	0.0125	0.0125	2.315800912037878	0.9860032076007205	48.09280080596852
Case 6.1.5	0.0125	0.0125	3.004283302198541	0.9847606913347033	41.42159866823076
Case 6.1.6	0.025	0.025	5.519520896140588	0.9804916164771977	15.56936805077945
Case 6.1.7	0.025	0.025	7.6129781181848	0.9806093675789447	13.71511944823688
Case 6.1.8	0.025	0.025	10.86315690956873	0.9803668713972701	11.86327696425435
Case 6.1.9	0.025	0.025	16.29059159714386	0.9800718066608986	10.23980977162735
Case 6.1.10	0.025	0.025	26.33869553245833	0.9802129067546791	9.042418195146764
Case 6.1.11	0.025	0.025	47.98116891173758	0.980293256909013	7.964013508962916

TABLE 8: Quenching data of b_x and b_y based on convection term $b/(\alpha x + \beta y)$.

Case name	x_{max}	y_{max}	T_{max}	max u	max u_t
Case 6.2.1	0.0625	0.0625	10.99093267786784	0.9804498472291583	8.583794969514605
Case 6.2.2	0.0375	0.0375	7.809655701953323	0.9804503193889351	12.7219405872281
Case 6.2.3	0.0375	0.0375	6.210534222541208	0.9809122863640634	13.14389285559599
Case 6.2.4	0.025	0.025	4.956004105630788	0.9818372265165442	18.9029625958216
Case 6.2.5	0.0125	0.0125	2.64799664630179	0.9810960736197033	31.29445994657764
Case 6.2.6	0.0125	0.0125	9.559656653594685	0.9813004101488958	33.42529207679014
Case 6.2.7	0.025	0.025	18.1622615973841	0.9808985418280476	18.03120629119135
Case 6.2.8	0.0375	0.025	38.77536139517031	0.9804090344629824	14.575573131335622
Case 6.2.9	0.0375	0.0375	59.07244177030795	0.9802503334133788	12.64186937140285
Case 6.2.10	0.0375	0.0375	89.05678402848356	0.9803538247671133	13.00866087970327

TABLE 9: Quenching data of α and β based on convection term $b/(\alpha x + \beta y)$.

Case name	x_{max}	y_{max}	T_{max}	max u	max u_t
Case 6.3.1	0.5375	0.5375	8.240022739766165	0.9805231629517244	19.33141003501417
Case 6.3.2	0.1229	0.1229	6.240792928817466	0.9804429759036448	21.02610806687704
Case 6.3.3	0.0625	0.0625	3.431334351295505	0.9809418101698555	21.77295829105509
Case 6.3.4	0.0375	0.0375	3.441737958890371	0.9816372001957696	23.0950930660414
Case 6.3.5	0.025	0.025	3.750551299221261	0.9801324957943957	19.04800266218939
Case 6.3.6	0.025	0.025	4.024152273164159	0.9800420381170325	17.6646128655794
Case 6.3.7	0.025	0.025	4.065155138423362	0.9805944201781043	18.01149509967014
Case 6.3.8	0.0125	0.0125	4.06558591278706	0.9807065134704962	30.77480165240926
Case 6.3.9	0.0125	0.0125	3.520143605280937	0.9809208903166006	24.6618068728011
Case 6.3.10	0.0125	0.0125	13.44243402330071	0.9805575860550446	8.352004051122194

and defined as $q = 0.8$, $b_x = b_y = -2$, $\alpha = \beta = \sqrt{11000}$. Tables 7–10 and Figures 6–9 demonstrate specific quenching information of Case 6.0.

The effect of q on quenching problem can be illustrated by continual experiments. A reasonable quenching behavior will occur when $q = 0$ or q takes a value in $[0.4, 1.4]$. When q is 0.1, 0.2, 0.3, or $q \geq 1.5$, it does not produce quenching phenomena. There are quenching characteristics for q:

quenching location x_{max} is not equal to y_{max} when q takes 0, 0.5 while x_{max} is equal to y_{max} in the other cases; (x_{max}, y_{max}) is $(0.0125, 0.0125)$ when q takes 0.6, 0.7, and 0.8; (x_{max}, y_{max}) is $(0.025, 0.025)$ when q is in $[0.9, 1.4]$. Quenching time T_{max} increases as q increases in the domain of q. Table 7 gives some of these quenching cases, in which Case 6.1.1 is $q = 0$, $b_x = b_y = -2$, $\alpha = \beta = \sqrt{11000}$; Case 6.1.2 is $q = 0.4$, $b_x = b_y = -2$, $\alpha = \beta = \sqrt{11000}$; Case 6.1.3 is $q = 0.5$, $b_x =$

TABLE 10: The maximal values and locations of u and u_t for $q = 0.8$, $b_x = b_y = -2$, $\alpha = \beta = \sqrt{11000}$ based on convection term $b/(\alpha x + \beta y)$.

| t	x	y	$\max_{x,y} u$	$\max_{x,y}(u_t)$
3.946999999999676	0.0125	0.0125	0.8195986394102188	2.499122191096586
3.999999999999671	0.0125	0.0125	0.8921719731921093	4.684299269080528
4.016999999999676	0.0125	0.0125	0.9488686925507734	10.88364621771482
4.019595682766669	0.0125	0.0125	0.9692844094996356	18.7880259490986
4.020449234557191	0.0125	0.0125	0.981186659892471	31.34049546140411
4.02068525061823	—	—	$5.358959032595640 \times 10^{16}$	$7.966445413263532 \times 10^{19}$

(a)

(b)
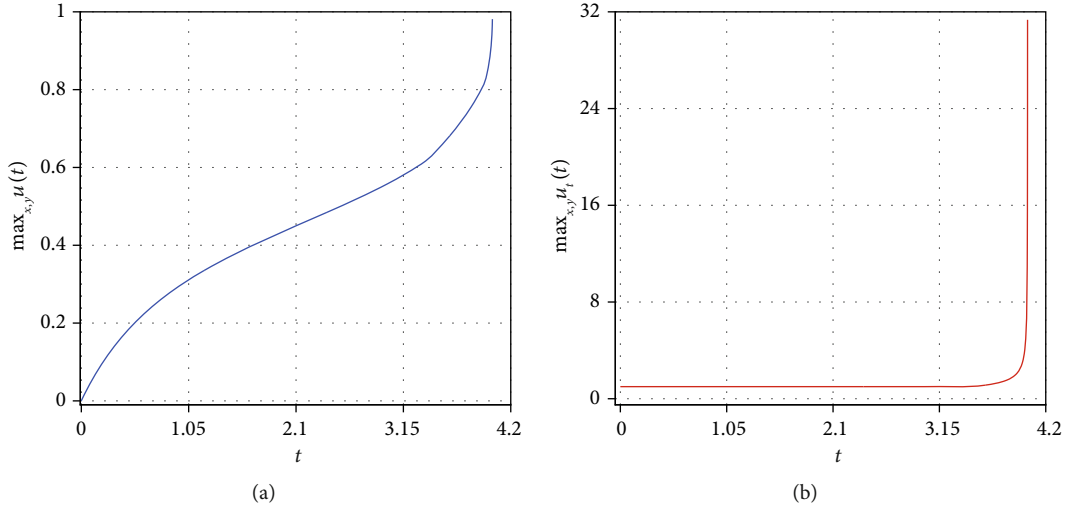
FIGURE 6: The graphs of solution u and u_t: (a) $\max_{x,y} u$ as t increases, and (b) $\max_{x,y}(u_t)$ as t increases from the initial time to the occurrence of quench behavior with $q = 0.8$, $b_x = b_y = -2$, $\alpha = \beta = \sqrt{11000}$ based on convection term $b/(\alpha x + \beta y)$.

$b_y = -2$, $\alpha = \beta = \sqrt{11000}$; Case 6.1.4 is $q = 0.6$, $b_x = b_y = -2$, $\alpha = \beta = \sqrt{11000}$; Case 6.1.5 is $q = 0.7$, $b_x = b_y = -2$, $\alpha = \beta = \sqrt{11000}$; Case 6.1.6 is $q = 0.9$, $b_x = b_y = -2$, $\alpha = \beta = \sqrt{11000}$; Case 6.1.7 is $q = 1$, $b_x = b_y = -2$, $\alpha = \beta = \sqrt{11000}$; Case 6.1.8 is $q = 1.1$, $b_x = b_y = -2$, $\alpha = \beta = \sqrt{11000}$; Case 6.1.9 is $q = 1.2$, $b_x = b_y = -2$, $\alpha = \beta = \sqrt{11000}$; Case 6.1.10 is $q = 1.3$, $b_x = b_y = -2$, $\alpha = \beta = \sqrt{11000}$; Case 6.1.11 is $q = 1.4$, $b_x = b_y = -2$, $\alpha = \beta = \sqrt{11000}$; Case 6.0 is between Case 6.1.5 and Case 6.1.6.

The paragraphs describe the relationship between $b_x(b_y)$ and quenching features. We write ten cases in Table 8. Case 6.2.1 is $q = 0.8$, $b_x = b_y = -16$, $\alpha = \beta = \sqrt{11000}$; Case 6.2.2 is $q = 0.8$, $b_x = b_y = -10$, $\alpha = \beta = \sqrt{11000}$; Case 6.2.3 is $q = 0.8$, $b_x = b_y = -7$, $\alpha = \beta = \sqrt{11000}$; Case 6.2.4 is $q = 0.8$, $b_x = b_y = -5$, $\alpha = \beta = \sqrt{11000}$; Case 6.2.5 is $q = 0.8$, $b_x = b_y = 1$, $\alpha = \beta = \sqrt{11000}$; Case 6.2.6 is $q = 0.8$, $b_x = b_y = 12$, $\alpha = \beta = \sqrt{11000}$; Case 6.2.7 is $q = 0.8$, $b_x = b_y = 21$, $\alpha = \beta = \sqrt{11000}$; Case 6.2.8 is $q = 0.8$, $b_x = b_y = 40$, $\alpha = \beta = \sqrt{11000}$; Case 6.2.9 is $q = 0.8$, $b_x = b_y = 57$, $\alpha = \beta = \sqrt{11000}$; Case 6.2.10 is $q = 0.8$, $b_x = b_y = 80$, $\alpha = \beta = \sqrt{11000}$; Case 6.0 is between Case 6.2.4 and Case 6.2.5. Quenching behavior can be formed when $b_x(b_y)$ takes the values in $[-16, 80]$, in which the function curve of $(b, T_{\max})$ is concave and $T_{\max}$ is smallest when

$b = 1$. When $b = -16$, $b = -13$, $b \in [-10, -7]$, $b \in [-5, 12]$, $b \in [21, 39]$, or $b \in [57, 80]$, quenching location $x_{\max}$ is equal to $y_{\max}$ whereas when b takes other values in $[-16, 80]$, $x_{\max}$ is different from $y_{\max}$.

We describe the influence of α and β on quenching results just depending on quenching data in Table 9. Of course, we do a great quantity of experiments, from which some typical cases chosen in Table 9. We set $\alpha/\beta = 1$ and α^2 from 10 to 3.0×10^6 for Cases 6.3.1-6.3.10. Specifically, Case 6.3.1 is $q = 0.8$, $b_x = b_y = -2$, $\alpha/\beta = 1$, $\alpha^2 = 10$; Case 6.3.2 is $q = 0.8$, $b_x = b_y = -2$, $\alpha/\beta = 1$, $\alpha^2 = 231$; Case 6.3.3 is $q = 0.8$, $b_x = b_y = -2$, $\alpha/\beta = 1$, $\alpha^2 = 1000$; Case 6.3.4 is $q = 0.8$, $b_x = b_y = -2$, $\alpha/\beta = 1$, $\alpha^2 = 2756$; Case 6.3.5 is $q = 0.8$, $b_x = b_y = -2$, $\alpha/\beta = 1$, $\alpha^2 = 8648$; Case 6.3.6 is $q = 0.8$, $b_x = b_y = -2$, $\alpha/\beta = 1$, $\alpha^2 = 10500$; Case 6.3.7 is $q = 0.8$, $b_x = b_y = -2$, $\alpha/\beta = 1$, $\alpha^2 = 10775$; Case 6.3.8 is $q = 0.8$, $b_x = b_y = -2$, $\alpha/\beta = 1$, $\alpha^2 = 10779$; Case 6.3.9 is $q = 0.8$, $b_x = b_y = -2$, $\alpha/\beta = 1$, $\alpha^2 = 19991$; Case 6.3.10 is $q = 0.8$, $b_x = b_y = -2$, $\alpha/\beta = 1$, $\alpha^2 = 300000$; Case 6.0 is between Case 6.3.8 and Case 6.3.9.

It does not form quenching status when $\alpha^2 < 10$ or $\alpha^2 < 3.0 \times 10^6$. After α/β is defined as 1, α^2 is evaluated from 10 to 3.0×10^6. We find that it is more likely to produce quenching behaviors when α^2 is between 10 and 3.0×10^6. By means of continual tests, Cases 6.3.1-6.3.10 represent
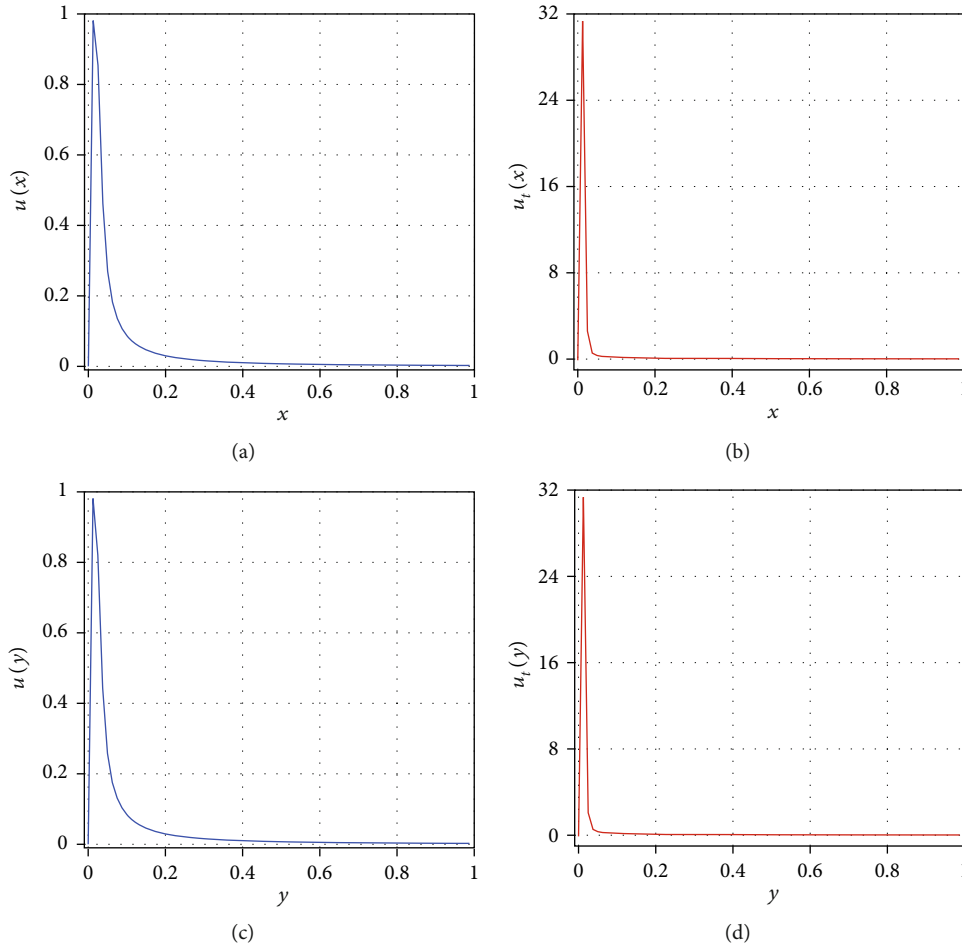
(a)

(b)

(c)

(d)

FIGURE 7: The graphs of (a) u as x increases, (b) u_t as x increases, (c) u as y increases, and (d) u_t as y increases when t is $T_5 *$ for convection term $b/(1 + \alpha x + \beta y)$.

the ten special cases, and we can observe the quenching status as follows. As far as quenching spatial characteristic is concerned, quenching location does not monotonously increase as α^2 increases when α^2 is in the definition domain. For example, quenching location reaches the maximum $(0.5375, 0.5375)$ when $\alpha^2 = 10$ and quenching location keeps the coordination point of $(0.0125, 0.0125)$ when α^2 is in $[10780, 3.0 \times 10^6]$. Next, quenching temporal characteristic is concerned. In fact, there does not exist strict linear relationship between quenching time and α^2. Comparatively, quenching time is smaller in the former half than in the latter half of the domain of α^2. When the measurement scale is enlarged in the domain of α^2, especially when α^2 reaches 19991, $T_{\max}$ increases with the increase of α^2.

Quenching phenomena of Case 6.0 can be considered in the following text. Its quenching time appears at $T_6 * = 4.020449234557191$, and its quenching position appears at $(x_6 *, y_6 *) = (0.0125, 0.0125)$ in this situation. Table 10 shows six stages around quenching for Case 6.0. The items from the first to the fifth describe the five stages of representation before the occurrence of quenching, and the last item just notes the quenching moment. $\max_{x,y} u$ is $5.358959032595640 \times 10^{16}$ at $(2.0588245639243 \times 10^{-4}, 9.654095827421034 \times 10^{-1})$, and

$\max_{x,y}(u_t)$ is $7.966445413263532 \times 10^{19}$ at $(2.080224198836234 \times 10^{-5}, 9.824584434865121 \times 10^{-1})$ when quenching occurs. A comprehensive statement of quenching states with the parameters $q = 0.8$, $b_x = b_y = -2$, $\alpha = \beta = \sqrt{11000}$ is recorded in the next paragraphs. Although there is slight perturbation in the left boundary of u_t, it does not influences on distribution of u_t. It is evident that Figures 6(a) and 6(b) give two pairs curves of both $\max_{x,y} u$ and $\max_{x,y}(u_t)$. The first one is for the distribution of the solution $\max_{x,y} u(t)$ as t varies, and the second one is for the distribution of $\max_{x,y} u_t(t)$ as t increases. There is small perturbation near the start-up of the adaptive procedure for the left figure of $\max_{x,y}(u_t)$. The four figures in Figure 7 give function relationship physical quantities between u, u_t, and spatial variables. Figure 7(a) paints the contour of (x,u), Figure 7(b) paints the contour of (x,u_t), Figure 7(c) paints the contour of (y,u), and Figure 7(d) paints the contour of (y,u_t). Similarly, Figures 7(a) and 7(c) have the same shape, and Figures 7(b) and 7(d) have the same shape.

There are three graphics in Figure 8, which represent three function relationships between spatial step in $x -$ direction and x, between spatial step in $y -$ direction and y,
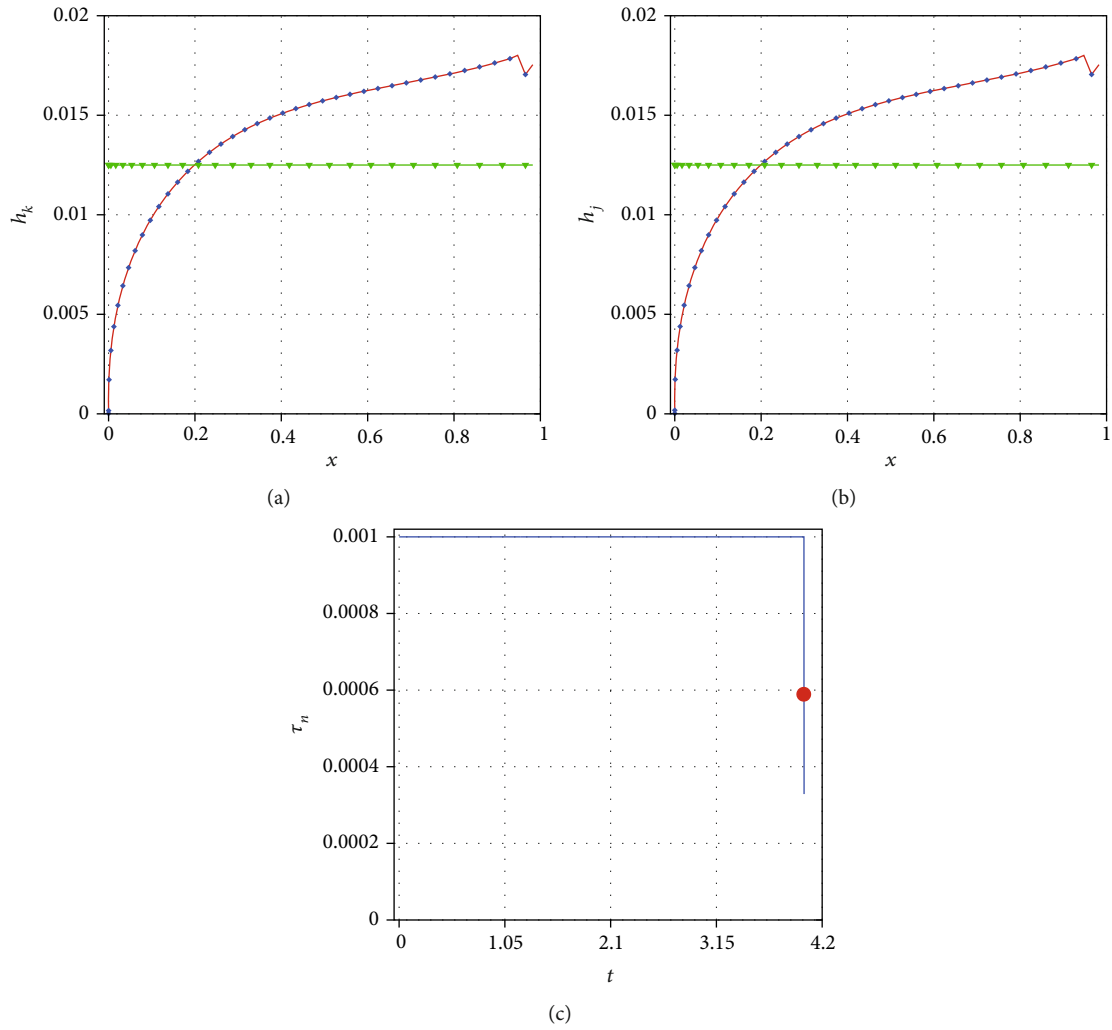
(a)

(b)

(c)

Figure 8: (a) The variation of spatial step h_k as space x processes; (b) the variation of spatial step h_j as space y processes; (c) the curve of the temporal steps τ_n as time t increases with the parameters $q = 0.8$, $b_x = b_y = -2$, $\alpha = \beta = \sqrt{11000}$ based on convection term $b/(\alpha x + \beta y)$.
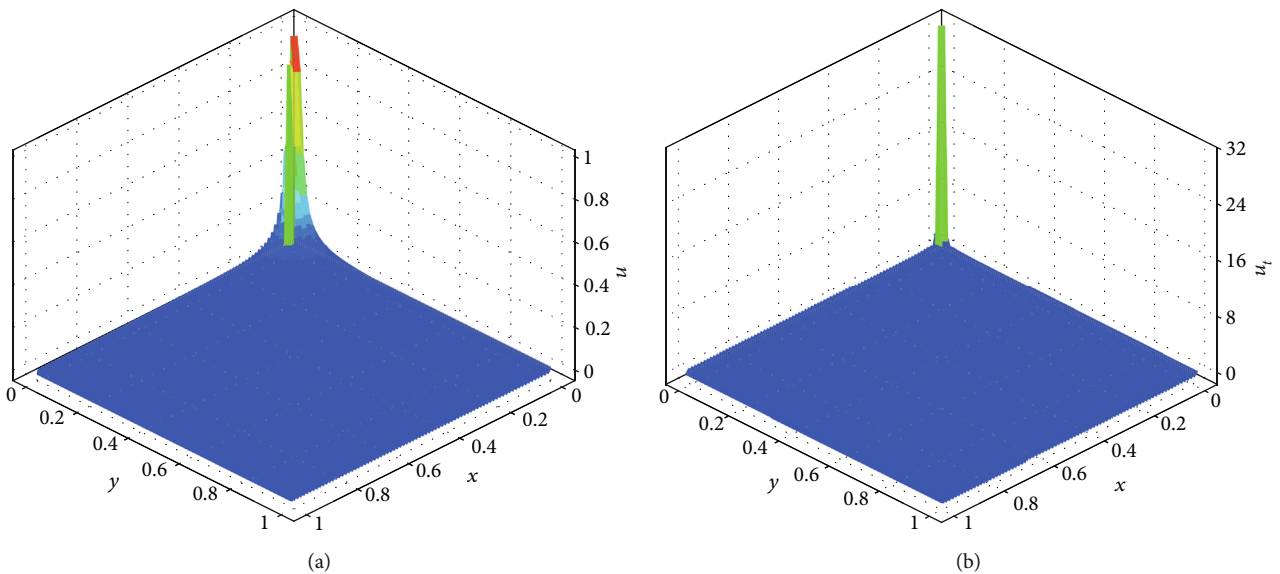

(a)

(b)

Figure 9: (a) The 3D plot of u when $t = T_6 *$ and (b) the 3D plot of u_t when $t = T_6 *$ for Case 6.0.

and between temporal step and t, respectively. Figure 8(a) depicts two curves, in which one is between initial spatial steps h_k and x, and another is between quenching spatial steps h_k and x. Figure 8(b) also describes two curves, in which one is between initial spatial steps h_k and y, and another is between quenching spatial steps h_k and y. The green lines with gradient marks reflect the initial spatial step distribution that is uniform regardless of x – direction or y – direction. The red curves covered by blue squares reflect quenching spatial steps that are self-adaptive when quenching occurs. There is a blue curve with a red square marks in Figure 8(c), which portrays temporal step τ_n varies as t changes from 0 to $T_6 *$. τ_n keeps 0.001 when $0 \leq t < 4.019595682766669$, but after τ_n becomes $5.956827669919562 \times 10^{-4}$ when $t = 4.019595682766669$ which signed as a red square, τ_n sharply declines up to $3.286760944343214 \times 10^{-4}$ when $t = T_6 *$.

The three-dimensional surfaces can render more reliable information for both the solution u and the time derivative u_t which display in Figure 9. The group of surfaces is the three-dimensional views of both u and u_t when t is equal to $T_6 *$. It is smooth and steady that the solution u carries forward at the temporal axis in Figure 9(a). Moreover, it is almost at the middle position of each time axis that the case gives birth to the peak value of u. When the position $(x_6 *, y_6 *)$ is at ($0.0125, 0.0125$) immediately before quenching occurs, the peak value of the solution approaches 1. The three-dimensional representation of Figure 9(b) reveals the evolution of the temporal derivative with regard to spatial variables. The temporal derivative of the solution varies smoothly and reaches its maximums at the quenching domain $(0.0125, 0.0125)$. At last, the temporal derivative becomes infinite when quenching occurs at another location $(2.080224198836234 \times 10^{-5}, \quad 9.824584434865121 \times 10^{-1})$, which is not observed in Figure 9(b). It is obvious for Case 6.0 that quenching occurs based on $\max_{x,y} u \longrightarrow 1^-$ and $\max_{x,y}(u_t) \longrightarrow 32^-$ as t reaches $T_6 *$.

5. Conclusion

Relying on the analyses in this paper, we can sort up the relationship between the parameters q, $b_x(b_y)$, $a(\beta)$, and quenching behaviors. There exist four aspects concluded as follows. First, the degenerate function acts within the normal range if the degeneracy parameter q is larger than or equal to 0.4 but not more than 1.3, and quenching time increases as q increases. Second, there is a special point $b^{\wedge}$ dividing the definition domain of convection parameter b as the left and the right subdomain, in which quenching phenomena occur normally and have a variety of features. Quenching time decreases as b increases in the left subdomain, and quenching time increases as b increases in the right subdomain. Quenching location either decreases or convergences upon a certain value as b increases in the domain of b. Third, under the condition of $\alpha/\beta = 1$, the influence of α^2 on quenching result is researched. There exists still a special point $\alpha^{\wedge}$ categorizing the definition domain of α^2 as two subdomains, in

which quenching phenomena occur normally and display different spatial effects. Specially, with the rise of α^2, quenching location does not increases monotonously in the left hand of $\alpha^{\wedge}$ and tends to a fixed coordinates in the right hand of $\alpha^{\wedge}$. Additionally, if we rely on a small scale to observe the domain of α^2, then there is no linear relationship between quenching time and α^2. We investigate the definition by virtue of a big scale to find that quenching time also increases when α^2 become larger, especially when α^2 reaches certain value; quenching time increases as α^2 rises. Fourth, it must be a good choice to set θ as 1. Through experiments, it is hard to produce quenching phenomena that can be formed when $\theta \geq 2$. From the result analyses, it can be discovered that it is meaningful to initially investigate the 2D singularity degeneracy problem of quenching type based on the unsteady convection-reaction-diffusion equation by using the high-order difference scheme, which will probably lead to the potentially support to research the next quenching problems.

Data Availability

The data used to support the findings of this study are available from the corresponding author upon request.

Conflicts of Interest

The authors declare that they have no conflicts of interest.

Acknowledgments

References

[1] K. S. Ha, R. J. Park, S. B. Kim, and H. D. Kim, "Experimental investigations of the quenching phenomena for hemispherical downward facing convex surfaces with narrow gaps," *International Communications in Heat and Mass Transfer*, vol. 34, no. 1, pp. 28–36, 2007.

[2] J. Lee, G. Son, and H. Y. Yoon, "Numerical simulation of the quenching process in liquid jet impingement," *International Communications in Heat and Mass Transfer*, vol. 61, pp. 146–152, 2015.

[3] H. Ramezanzadeh, A. Ramiar, and M. Yousefifard, "Numerical investigation into coolant liquid velocity effect on forced convection quenching process," *Applied Thermal Engineering*, vol. 122, pp. 253–267, 2017.

[4] J. Q. Li, L. W. Mou, J. Y. Zhang, Y. H. Zhang, and L. W. Fan, "Enhanced pool boiling heat transfer during quenching of water on superhydrophilic porous surfaces: effects of the surface wickability," *International Communications in Heat and Mass Transfer*, vol. 125, pp. 494–505, 2018.

[5] F. Yokomatsu, W. Fogaça, S. Mori, and M. Tanaka, "On the quenching of stainless steel rods with a honeycomb porous

plate on a nanoparticle deposited surface in saturated water," *International Journal of Heat and Mass Transfer*, vol. 127, pp. 507–514, 2018.

[6] R. Z. Xu, C. Y. Jin, T. Yu, and Y. C. Liu, "On quenching for some parabolic problems with combined power-type nonlinearities," *Nonlinear Analysis: Real World Applications*, vol. 13, no. 1, pp. 333–339, 2012.

[7] S. M. Zhou, C. L. Mu, Q. L. Du, and R. Zeng, "Quenching for a reaction–diffusion equation with nonlinear memory," *Communications in Nonlinear Science Numerical Simulation*, vol. 17, no. 2, pp. 754–763, 2012.

[8] H. Pan and R. Xing, "Fringing field can prevent infinite time quenching," *Nonlinear Analysis: Real World Applications*, vol. 30, pp. 126–142, 2016.

[9] J. Zhou, "Quenching for a parabolic equation with variable coefficient modeling MEMS technology," *Applied Mathematics and Computation*, vol. 314, pp. 7–11, 2017.

[10] Q. Wang, "Quenching phenomenon for a parabolic MEMS equation," *Chinese Annual of Mathematics Series B*, vol. 39, no. 1, pp. 129–144, 2018.

[11] S. M. Zhou and C. L. Mu, "Quenching for a reaction-diffusion system with coupled inner singular absorption terms," *Boundary Value Problems*, vol. 2010, no. 1, Article ID 797182, p. 15, 2010.

[12] B. Selcuk, "Quenching behavior of a semilinear reaction-diffusion system with singularboundary condition," *Turkish Journal of Mathematics*, vol. 40, pp. 166–180, 2016.

[13] I. D. Bonis and A. Muntean, "Existence of weak solutions to a nonlinear reaction-diffusion system with singular sources," *Electronic Journal of Differential Equations*, vol. 2017, no. 202, pp. 1–16, 2017.

[14] B. Selcuk and N. Ozalp, "The quenching behavior of a semilinear heat equation with a singular boundary outflux," *Quarterly of Applied Mathematics*, vol. 72, no. 4, pp. 747–752, 2017.

[15] Y. Ge, Z. Cai, and Q. Sheng, "A compact adaptive approach for degenerate singular reaction-diffusion equations," *Numerical Methods in Partial Differential Equations*, vol. 34, no. 4, pp. 1166–1187, 2018.

[16] M. A. Beauregard, "Numerical approximations to a fractional Kawarada quenching problem," *Applied Mathematics and Computation*, vol. 349, pp. 14–22, 2019.

[17] Q. Zhou, Y. Y. Nie, X. Zhou, and W. Guo, "Quenching of a semilinear diffusion equation with convection and reaction," *Electronic Journal of Differential Equations*, vol. 2015, no. 208, pp. 1–7, 2015.

[18] X. Zhu and R. Hong, "High-order compact difference scheme of 1D nonlinear degenerate convection–reaction–diffusion equation with adaptive algorithm," *Numerical Heat Transfer, Part B: Fundamentals*, vol. 75, no. 1, pp. 43–66, 2019.

[19] M. A. Beauregard and Q. Sheng, "A semi-adaptive compact splitting method for the numerical solution of 2-dimensional quenching problems," *Applied Mathematics and Computation*, vol. 218, no. 22, pp. 11240–11254, 2012.

[20] M. A. Beauregard and Q. Sheng, "Solving degenerate quenching-combustion equations by an adaptive splitting method on evolving grids," *Computers and Structures*, vol. 122, pp. 33–43, 2013.

[21] J. L. Padgett and Q. Sheng, "Numerical solution of degenerate stochastic Kawarada equations via a semi-discretized approach," *Applied Mathematics and Computation*, vol. 325, pp. 210–226, 2018.

[22] X. Zhu and Y. Ge, "Adaptive ADI numerical analysis of 2D quenching-type reaction: diffusion equation with convection term," *Mathematical Problems in Engineering*, vol. 2020, Article ID 8161804, 19 pages, 2020.

[23] S. H. Kwang, J. P. Rae, B. K. Sang, and D. K. Hee, "A high-accuracy finite difference scheme for solving reaction-convection-diffusion problems with a small diffusivity," *Advances in Applied Mathematics and Mechanics*, vol. 6, no. 5, pp. 637–662, 2014.

[24] L. Li, Z. Jiang, and Z. Yin, "Fourth-order compact finite difference method for solving two-dimensional convection–diffusion equation," *Advances in Difference Equations*, vol. 234, 24 pages, 2018.

[25] L. Wu and S. Zhai, "A new high order ADI numerical difference formula for time-fractional convection-diffusion equation," *Applied Mathematics and Computation*, vol. 7, pp. 1–10, 2019.

[26] W. Xue and Y. Ge, *High-order compact difference schemes and multigrid algorithms on non-uniform grids for the two-dimensional incompressible vorticity-stream function Navier-Stokes equations*, Ningxia University, Yinchuan, 2014.

[27] X. Huang and Y. Ge, *A high-order compact ADI method on non-uniform grid for unsteady convection-diffusion equations*, Ningxia University, Yinchuan, 2013.